land

MDPI

Article

Spatial Identification and Change Analysis of Production-Living-Ecological Space Using Multi-Source Geospatial Data: A Case Study in Jiaodong Peninsula, China

Mingyan Ni [1], Yindi Zhao [1,*], Caihong Ma [2], Wenzhi Jiang [1], Yanmei Xie [1,2] and Xiaolin Hou [1,2]

[1] School of Environment and Spatial Informatics, China University of Mining and Technology, Xuzhou 221116, China; nimy@cumt.edu.cn (M.N.)
[2] Aerospace Information Research Institute, Chinese Academy of Sciences, Beijing 100094, China; mach@aircas.ac
* Correspondence: zhaoyd@cumt.edu.cn

Abstract: The significant heterogeneity in the spatial distribution of point of interest (POI) data, the absence of human socio-economic activity information in remote sensing images (RSI), and the high cost of land use (LU) data acquisition restrict their application in PLES spatial identification. Utilizing easily accessible data for detailed spatial identification of PLES remains an urgent challenge, especially when selecting a study area that encompasses both urban built-up areas (UBUA) and non-urban built-up areas (NUBUA). To address this issue, we proposed a PLES spatial identification method that combines POI data and land cover (LC) data in this paper. The proposed method first classified spatial analysis units (SAUs) into agricultural production space (APS), ecological space (ES), and ambiguous space (AS) based on the rich surface physical information from LC data. Subsequently, the AS was further classified into living space (LS) and non-agricultural production space (NAPS) based on the rich human socioeconomic information from POI data. For the AS that contains no POI, a simple rule was established to differentiate it into LS or NAPS. The effectiveness of the method was verified by accuracy evaluation and visual comparison. Applying the method to the Jiaodong Peninsula, we identified the PLES of the Jiaodong Peninsula for 2018 and 2022, further explored their spatial distribution characteristics, and analyzed their changes. Finally, we conducted a discussion on the real-world situations and driving mechanisms of the PLES changes and proposed several policy insights. The results indicated that both the spatial distribution characteristics of PLES and PLES change in the Jiaodong Peninsula were obvious and showed significant differentiation between UBUA and NUBUA. Climatic and natural resource conditions, geographic location, macro-policies, and governmental behaviors drove the PLES changes.

Keywords: land cover data; point of interest data; production-living-ecological space; regional land use/cover change; urban-rural difference

Citation: Ni, M.; Zhao, Y.; Ma, C.; Jiang, W.; Xie, Y.; Hou, X. Spatial Identification and Change Analysis of Production-Living-Ecological Space Using Multi-Source Geospatial Data: A Case Study in Jiaodong Peninsula, China. *Land* **2023**, *12*, 1748. https://doi.org/10.3390/land12091748

Academic Editor: Mateus Batistella

Received: 2 August 2023
Revised: 19 August 2023
Accepted: 28 August 2023
Published: 8 September 2023

1. Introduction

As a spatial carrier of human activities, land not only has the most basic survival resources and production factors for social and economic development but also has the function of maintaining an ecological balance between climate, soil, hydrology, and vegetation [1]. Production-living-ecological functions (PLEF) are the three aspects of land use function [2]. Production-living-ecological space (PLES), including production space (PS), living space (LS), and ecological space (ES), reflects the multifunctionality of land use, which is the basic carrier of human economic and social development [3]. In 2012, China proposed a development vision of intensive and efficient PS, livable and moderate LS, and unspoiled and beautiful ES [4]. Since then, achieving coordinated and sustainable development of PLES has become a major goal for the Chinese government in spatial planning system establishment, land allocation optimization, and ecological civilization

construction [3–5]. The dominant function conversion of land among production function, living function, and ecological function is one of the manifestations of land use change [6]. Urbanization and land use changes led to significant regional changes in the PLES spatial pattern [7]. Exploring regional changes in the PLES is of great significance for optimizing the spatial allocation of regional resources. This will promote high-quality and sustainable development in the region.

Rapid and accurate identification of PLES is the basis for exploring the characteristics of PLES change. The existing related research used quantitative measurement and land use consolidation methods primarily to identify PLES [5,8]. By constructing an Evaluation Index System (EIS) to quantitatively measure the PLEF of land, the quantitative measurement method could identify PLES based on a series of socio-economic statistical data. For instance, Yang et al. [2] constructed an EIS containing 15 indicators to reveal the coordination of the PLES in the rural areas of the Beijing-Tianjin-Heibei region. This method takes sufficient account of the characteristics of the study area when constructing the EIS and evaluates the PLEF of land from multiple dimensions. However, the construction of the EIS is cumbersome, and the socioeconomic statistical data have problems such as low spatial resolution, low update frequency, and a strong time lag, which makes the application of this method to fine-grained research challenging [9]. Compared to the quantitative measurement method, the LU consolidation method is simpler and easier to implement [10]. It identifies the PLES by establishing the mapping relationship between LU types and PLES types. The existing PLES-related studies utilizing LU data [2–4,6,7,10,11] primarily obtained LU data through on-site investigations as well as by requesting land use data products from institutions. For instance, Duan et al. [1] used participatory mapping based on RSI to obtain LU data. The large number of on-site investigations undoubtedly leads to expensive time and labor costs. Gao et al. [11], on the other hand, used the LU data products published by the Chinese Academy of Sciences, which are generated through manual visual interpretation based on RSI [12]. The significant involvement of manual labor has led to escalated data acquisition costs and prolonged update intervals, rendering users unable to access the LU data products freely and promptly.

Benefiting from the abundant surface physical information provided by RSI, several scholars tried to acquire LU data based on RSI. For instance, Tao et al. [13] employed long-term RSI spanning the years 1975 to 2020 to acquire LU data for five resource-based cities and subsequently utilize the LU data to spatially identify PLES. However, the lack of human socioeconomic information limits the number of land use types that can be identified by RSI [14–16]. This limitation results in the inability of the method to accurately and comprehensively identify PS and LS, which further leads to a potential precision loss in results. While such precision loss is acceptable in resource-based cities dominated by industrial activities, it may be unacceptable in other urban contexts, especially in cities where the primary industry revolves around commercial and service sectors. In contrast to LU, land cover (LC) indicates physical land types and can be directly derived from RSI [17]. Automated LC mapping methods based on RSI were extensively developed [18–20], and several institutions also published freely accessible LC data products [21]. The convenience of LC data acquisition piqued scholars' interest in its application to PLES spatial identification. Li et al. [22] utilized RSI to obtain LC data and identified PLES by establishing a mapping relationship between LC types and PLES types. Similar to the method solely reliant on RSI, this method also faces challenges in accurately and comprehensively identifying PS and LS due to the lack of human socioeconomic activity information.

Social sensing data, represented by point-of-interest (POI) data, has the advantages of furnishing both geographic and spatial information and rich socioeconomic insights. The POI data provide new data support for revealing the urban internal spatial structure and urban human activity patterns and have been widely used in fine-scale urban studies, such as functional zone identification [23,24], urban boundary extraction [25,26], and land use mapping [27,28]. Based on POI data, Fu et al. [29] used the analytic hierarchy process,

spatial superposition method, and quadrat ratio method to identify the PLES in the central urban area of Wuhan City. Yang et al. [5] constructed a two-level scoring evaluation model for POI data to identify PLES in the main urban area of Hangzhou City. These studies have validated the efficacy and potential of POI data in PLES spatial identification. However, a strong heterogeneity is shown in the spatial distribution of POI data [30]. Due to significant differences in the intensity of human socioeconomic activities, POIs are more densely distributed in urban built-up areas (UBUA) and sparsely distributed in non-urban built-up areas (NUBUA) [31]. The strong heterogeneity hinders the application of POI data in NUBUA, and the results of the studies using POI data were mainly focused on UBUA.

Combining multi-source data can effectively break through the limitations of using a single data source. RSI and POI data were combined to apply to urban studies such as functional zone mapping [24], building function identification [32], and population mapping [33]. In terms of combining multi-source data for PLES spatial identification, Zhao et al. [34] combined POI data, LU data, taxi trajectory data, and area of interest data to spatially identify PLES in the central area of Haikou City. Fu et al. [35] employed high-resolution RSI, building vector data, POI data, and nighttime lighting data to spatially identify PLES in the urban region of Ningbo City. These studies effectively identify PLES in detail by fusing surface physical and socioeconomic information from multi-source data. However, these methods have not effectively addressed the issues that limit the application of POI data in NUBUA. Due to the significant discrepancies in development degree, production mode, and land planning, significant differences exist in the LU mode between UBUA and NUBUA [36]. These differences are reflected in the function and landscape of the land, reflecting the differences between UBUA and NUBUA in economic activities, human settlement environment, and ecological quality. Therefore, including the NUBUA in the study area is helpful for policymakers to sufficiently understand the overall development in the region, which is meaningful for the promotion of regionally coordinated development.

Overall, with the selection of a region including UBUA and NUBUA as a study area, how to use easily accessible data to spatially identify PLES in detail is still an urgent problem to be solved. To address this issue, we proposed a method for the spatial identification of regional PLES that combines POI data and LC data in this study. The method combines the strengths of POI data and LC data while considering the differences between UBUA and NUBUA. By applying the proposed method, we spatially identified the PLES in Jiaodong Peninsula for 2018 and 2022, and the change areas were obtained by spatial overlay analysis. Based on the results, we analyzed the spatial distribution characteristics of PLES and PLES change. Through the exploration and discussion of the real-world situations and driving mechanisms of the PLES changes, policy implications were proposed.

The outline of the rest of this paper is organized as follows: Section 2 introduces the study area, data sources, and methodology. Section 3 presents the results of PLES identification and analyzes the spatial distribution characteristics of PLES and their changes. Section 4 delves into the real-world situation and driving mechanisms of the PLES changes and proposes policy implications. Additionally, this section also discusses the advantages of the proposed method and the limitations and prospects of this study. Section 5 concludes this paper by summarizing the results and discussions. Abbreviations provides a compilation of acronyms in this paper.

2. Materials and Methods

In this study, the PLES was identified from the perspective of the dominant function of land. According to the definition of the PLES, the PS refers to the specific functional area where people engage in production activities; the LS carries the residence, consumption, leisure, and entertainment of residents; and the ES refers to the area that can provide ecological products and ecological services with ecological protection functions [2,29,37]. Due to the significant differences between agricultural production and non-agricultural production in production methods, land use, and ecological impacts, the PS is

further divided into agricultural production space (APS) and non-agricultural production space (NAPS).

2.1. Study Area

As shown in Figure 1, the Jiaodong Peninsula is located in the eastern coastal area of Shandong Province, adjacent to the Bohai Sea and the Yellow Sea. The Jiaodong Peninsula is a vast area, including the cities of Qingdao, Yantai, and Weihai, with a total land area of 30,645.95 km^2, accounting for 19% of Shandong Province. The Jiaodong Peninsula is rich in marine resources, with a coastline length of 2711.88 km, accounting for about 74% of the coastline length of Shandong Province. Meanwhile, Jiaodong Peninsula is also an important production base for fruit, grain, and aquatic products in Shandong Province. Thanks to its unique location advantages, Jiaodong Peninsula has a strong economy, with a gross domestic product (GDP) of 278.447 billion Chinese yuan (CNY) in 2022, accounting for about 32% of Shandong Province, and a permanent resident population of 20.319 million, accounting for about 20% of Shandong Province.

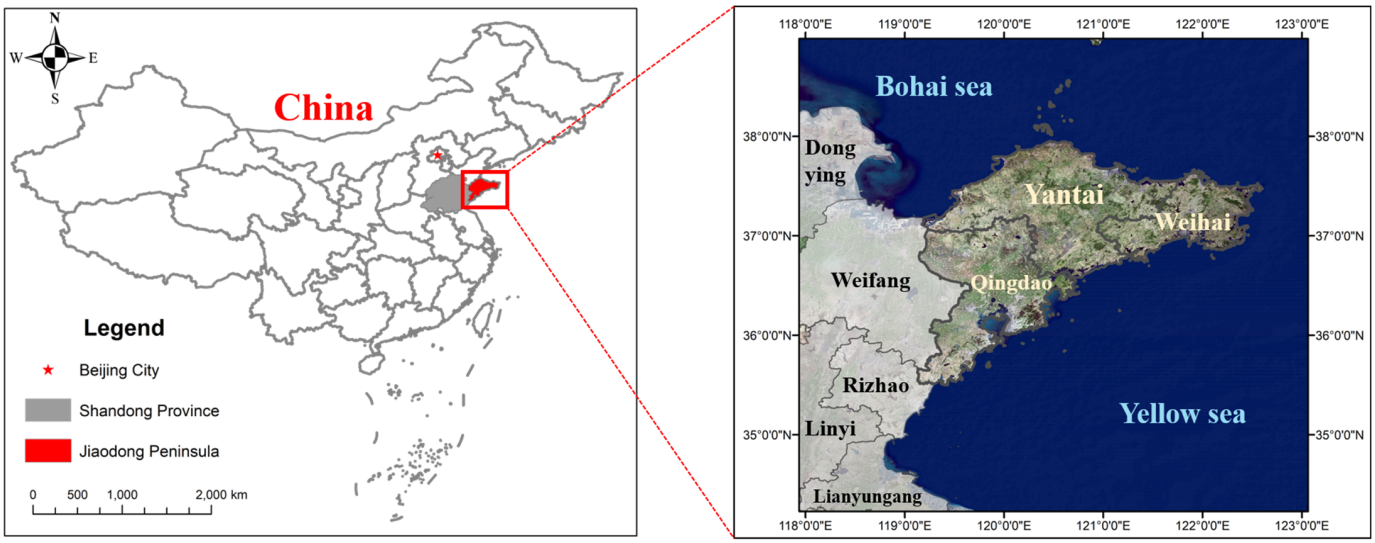

Figure 1. The location of the Jiaodong Peninsula.

Behind the rapid socioeconomic development, the expansion of built-up areas, resource production, land reclamation, and other human activities have led to significant changes in the landscape pattern of the PLES in the Jiaodong Peninsula. The conflicts and contradictions among the PLES in the Jiaodong Peninsula have become more and more prominent. Exploring the dynamic characteristics of PLES in the Jiaodong Peninsula is of great significance for optimizing the allocation of regional spatial resources and promoting high-quality and sustainable development in the region.

The Jiaodong Peninsula area contains several offshore islands, such as Chang Island, Liugong Island, and Jiming Island. Due to the low intensity of human activities and good habitat on the offshore islands, only the land area of the Jiaodong Peninsula was considered in this study.

2.2. Data Source and Preprocessing

The POI data for 2018 and 2022 were obtained from Amap via the application program interface (API). The annual road network data for 2018 and 2022 was downloaded from the Open Street Map (OSM) data platform. The LC data for 2018 and 2022 published by ESRI was used in this study, which was generated by a deep learning land classification model using billions of training pixels with an accuracy of more than 80% [38]. To avoid confusion with UBUA, we refer to the type named "built area" in the LC data as "construction land" in the following.

Construction land is the result of urbanization and industrialization and carries the daily lives of residents and non-agricultural economic activities, while non-construction land is mainly used for agricultural production, ecological protection, and environmental maintenance. Based on the definition of the PLES, the LC types were reclassified, and the mapping relationship between the LC types and PLES types was established. The reclassification results and the mapping relationship are shown in Table 1. Among them, the construction land and bare land have no clear dominant function and were temporarily reclassified into Ambiguous Space (AS).

Table 1. Reclassification results of LC data and mapping relationship between LC types and the types of PLES.

Original Type	Reclassified Type	Classification of PLES
Construction land	Construction land	Ambiguous space
Bare land	Bare land	Ambiguous space
Cropland	Cropland	Agricultural production space
Trees Rangeland Flooded vegetation	Vegetation	Ecological space
Water	Water	Ecological space

After data cleansing and coordinate transformation, the obtained POI data was reclassified based on the definition of the PLES and relevant national standards, including "Current land use classification" (GB/T 21010-2017) and "Code for classification of urban and rural land use and planning standards of development land" (GB 50137-2019). The reclassification results are shown in Table 2. The definition of the two reclassified types in Table 2 can be found in the two relevant national standards mentioned above.

Table 2. Reclassification results of POI data.

Reclassified Type I		Reclassified Type II		Original Type
Code	**Name**	**Code**	**Name**	**Name**
1	Residential	11	Residential	Villa, residential quarter, etc.
2	Public Administration and public service	21	Governmental organization and social group	Governmental organization, social group, public security organization, etc.
		22	Science, culture and education service	School, training institution, research institution, etc.
		23	Medical and healthy care service	Hospital, special hospital, plastic surgery, clinic, etc.
		24	Public facility	Public toilet, emergency shelter, etc.
3	Commercial service	31	Finance and insurance service	securities company, insurance company, automatic teller machine (ATM), bank, etc.
		32	Food and beverages	Restaurant, coffee house, bakery, teahouse, etc.
		33	Shopping service	Shopping plaza, home building materials market, convenience store, supermarket, etc.
		34	Daily life service	Ticket office, post office, telecom office, beauty and hairdressing store, etc.
		35	Auto service	Filling station, auto dealers, auto repair, etc.
		36	Motorcycle service	Motorcycle sales, motorcycle repair, etc.
		37	Sports and recreation	Sports stadium, theatre and cinema, holiday and nursing resort, recreation center, etc.
		38	Accommodation Service	Hotel, hostel, etc.
4	Industry-related	41	Enterprise	Enterprise, company, etc.
		42	Factory and industrial park	Factory, industrial park, etc.
		43	Business Office Building	Business office building, etc.
		44	Farming, forestry, animal husbandry, and fishery base	Farm, fishing farm, forest farm, flower nursery base, etc.

Table 2. *Cont.*

Reclassified Type I		Reclassified Type II		Original Type
Code	**Name**	**Code**	**Name**	**Name**
5	Transportation	51	Road furniture	Toll gate, expressway service area, etc.
		52	Transportation service	Railway station, bus station, port, marina, etc.
6	Scenic tourism	61	Tourist attraction	Memorial hall, beach, scenery spot, etc.
		62	Park and square	City plaza, park, square, zoo, etc.

2.3. UBUA Extraction and Spatial Analysis Unit Division

2.3.1. UBUA Extraction

According to the national standard "Standard for Terminology of Urban Planning" (GB/T 50280-98), the UBUA was defined as the area that has actually been continuously developed and constructed, where municipal utilities and public facilities are basically available. Traditionally, the extraction of UBUA is mostly based on remote sensing products, such as panchromatic images, multispectral images, and nighttime lighting data [39]. The arrival of the big data era has brought new data and methods for UBUA extraction. Xu et al. [25] proposed a method named Densi-Graph to extract UBUA by analyzing the kernel density contour of POI data. The extraction process of Densi-Graph is relatively simple and easy, and it can quickly carry out the extraction of UBUA. However, the method is based on kernel density contours and ignores the surface physical characteristics of UBUA, resulting in overly smooth boundaries in the extraction results [40]. Therefore, we used non-construction land to refine the boundaries of the initial UBUA extraction results obtained by using the Densi-Graph method. Specifically, the initial UBUA extraction results were first obtained by using the Densi-Graph method, then the initial results were erased by utilizing non-construction land vector data, and the final UBUA extraction results were obtained by filling the holes inside the erased initial results.

2.3.2. Spatial Analysis Unit Division

The division of the Spatial Analysis Unit (SAU) is a key step in fine-grained regional research. Currently, regular geographic grids and blocks are commonly used as SAUs. Previous studies prioritized regular geographic grids as the SAU [5,29] because of their advantages, such as simple construction, flexible spatial scale, and comparability with identical morphologies [41]. However, the significant heterogeneity of land use hinders the accurate representation of complex surface environments in regular grids [24]. In addition, the scale choice of regular geographic grids is crucial, and scale effects may lead to different results appearing in SAUs at different scales [5].

In recent years, as the coverage and quality of road network data provided by OSM have been improving year by year [42], many scholars have utilized irregular blocks segmented by road network data as SAUs [43,44]. However, similar to the POI data, a strong spatial heterogeneity was shown in the road network data provided by OSM [31], which makes it challenging to use the road network data alone for the SAU division. In addition, the functional differences between different road segments cannot be ignored [45]. One of the basic assumptions of spatial theory is stated in Tobler's first law of geography: "Everything is related to everything else, but near things are more related than distant things" [46,47]. Based on this, the PLEF of a road segment was considered to be dependent on the PLEF of its adjacent block in this study. Specifically, we divided SAUs using the centerline of the road. The purpose of adopting this division method is to consider the correlation between the PLEF of the road and the adjacent block while ensuring the adjacency of adjacent blocks in spatial topological relationships, which facilitates the construction of spatial weight matrixes in the subsequent spatial autocorrelation analysis.

In summary, in this study, based on the UBUA extraction results, irregular blocks segmented by road network data were used as the SAUs in the UBUA, and the regular geographic grids were used as the SAUs in the NUBUA. The size of the regular geographic

grids was set to 1 km × 1 km by referring to the literature [10,48] and taking into account the actual situation.

2.4. PLES Identification

2.4.1. Rating and Scoring System for POI Data

Based on the previous studies [2,5,49] and the investigations for Jiaodong Peninsula based on RSI, the Rating and Scoring System (RSS) for POIs was constructed after several experiments (Table 3). The RSS consists of an area-based score and a function-based score, in which the area-based scores were obtained by rating and scoring based on the average physical area of POIs in different types, with a range of 0 to 100. According to the PLEF strength of the different types of POIs, the function-based scores were obtained by dividing the POIs into four grades of strong function, general function, weak function, and no function with scores of 5, 3, 1, 0, respectively.

Table 3. Rating and scoring system for POI data.

Reclassified Type II [1]		Area-Based Score		Function-Based Score					
Code	Name	Average Physical Area (hm^2)	Area Score	Production Function Score [2]		Living Function Score		Ecological Function Score	
				UBUA	NUBUA	UBUA	NUBUA	UBUA	NUBUA
11	Residential	2	40	0	0	5	5	0	0
21	Governmental organization and social group	1.5	30	1	1	5	5	0	0
22	Science, culture, and education service	1.5	30	3	1	5	5	0	0
23	Medical and healthy care service	0.5	10	3	1	5	5	0	0
24	Public facility	0.1	2	0	0	5	5	0	0
31	Finance and insurance service	1	20	5	5	1	1	0	0
32	Food and beverages	0.5	10	3	3	5	5	0	0
33	Shopping service	1.5	30	5	3	3	5	0	0
34	Daily life service	0.5	10	1	1	5	5	0	0
35	Auto service	0.5	10	3	3	3	3	0	0
36	Motorcycle service	0.5	10	3	3	3	3	0	0
37	Sports and recreation	1	20	1	1	5	5	0	0
38	Accommodation Service	1	20	3	3	3	3	0	0
41	Enterprises	1	20	5	5	0	0	0	0
42	Factory and industrial park	5	100	5	5	0	0	0	0
43	Business Office Building	3	60	5	5	0	0	0	0
44	Farming, forestry, animal husbandry, and fishery base	2	40	3	3	0	0	3	3
51	Road furniture	2	40	3	3	3	3	0	0
52	Transportation service	1	20	3	3	3	3	0	0
61	Tourist attraction	5	100	0	0	1	1	5	5
62	Park and square	4	80	0	0	3	3	5	5

[1] The reclassified type II in this table corresponds to the reclassified type II in Table 2. [2] The production function score for the type coded 44 refers to agricultural production function, and the production function scores for the other types refer to non-agricultural production function.

Based on the differences between UBUA and NUBUA, including the differences in the styles of production and living and the differences in the spatial distribution of the POI data, the three types of POIs, namely, "Science, culture, and education service (SCES)", "Medical and Healthy Care Service (MHCS)", and "Shopping Service (SS)", were assigned different function-based scores. In NUBUA, the majority of POIs in the SCES type were POIs of public basic education, such as primary and secondary schools, which show a significant living function. In contrast, in UBUA, besides public basic education, the POIs

of SCES showed a wider range, including extra-curricular tutorial organizations, training institutions, and other types with more significant production functions. Similarly, the MHCS within NUBUA were mostly for public healthcare, while those within UBUA include beauty salons, plastic surgery, and other types that have a more production function. For SS, the SS within UBUA showed more commercial function, that is, the production function was more prominent, while the POIs of SS within NUBUA were mainly convenience stores, which mainly serve the daily lives of residents in NUBUA.

Based on the area-based score and the function-based score, the final score of each type of POI was calculated using the geometric mean method [50] with the following formula:

$$S_i = \sqrt{S_{ia} \times S_{if}} \quad (1)$$

where S_i is the final score of the i-th POI type, S_{ia} is the area-based score of the i-th POI type, and S_{if} is the function-based score of the i-th POI type.

2.4.2. Spatial Identification of PLES Based on LC Data and POI Data

The spatial identification process of PLES in this study is shown in Figure 2, and the detailed steps are as follows:

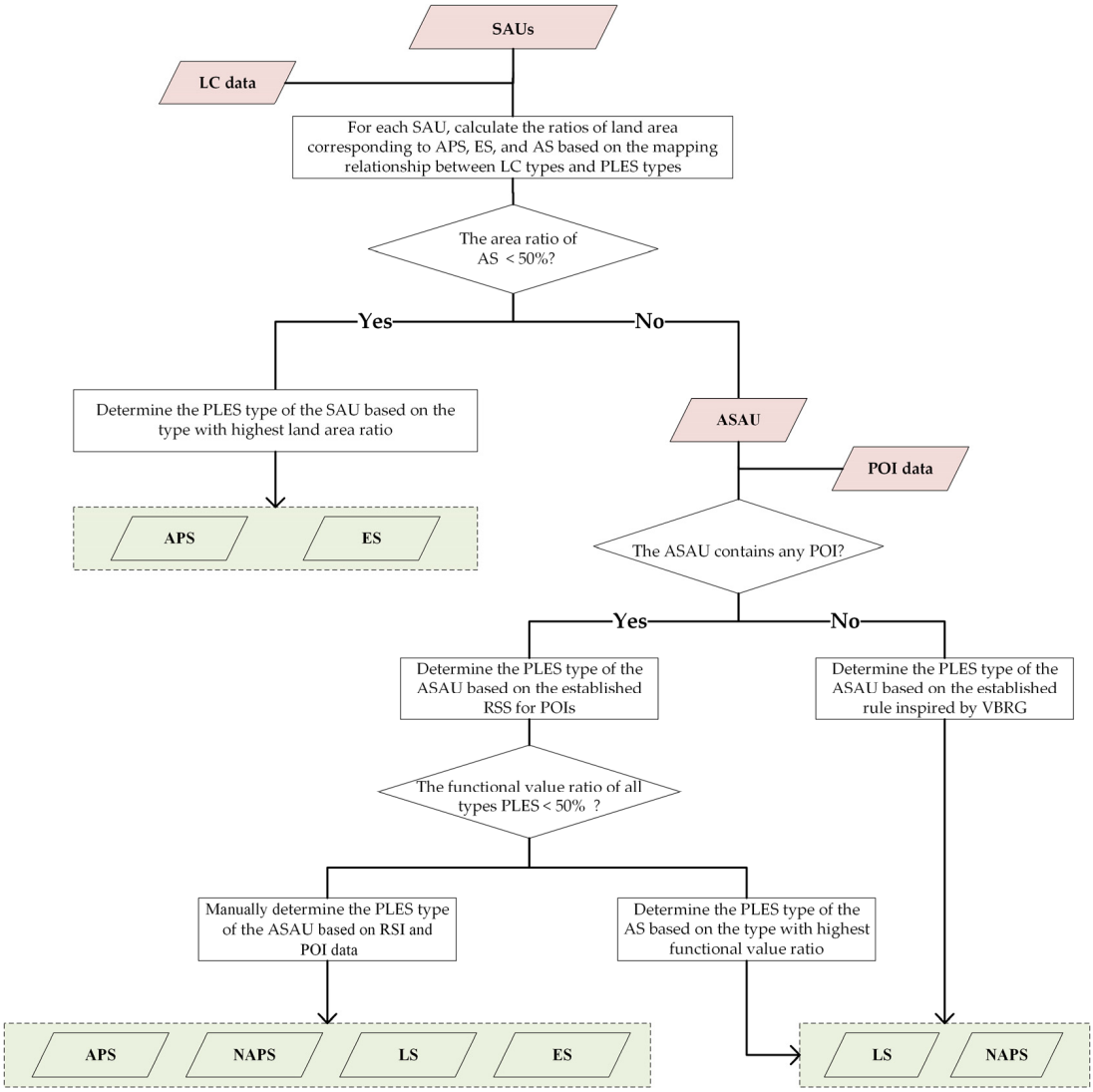

Figure 2. Illustration of the spatial identification process of PLES.

Step 1: Based on Table 1, the LC data were used to calculate the ratios of land area corresponding to APS, ES, and AS in each SAU. If the ratio of AS was less than 50%, then the SAU was identified as the PLES type corresponding to the type with the highest ratio in the calculation result. Otherwise, the SAU was defined as an ambiguous SAU (ASAU), and POI data were used for the next step to determine the PLES type of ASAU.

Step 2: Based on the final scores of the POI data for each type, the POI data were used to calculate the functional values in each ASAU, and subsequently, the ratio of each type of functional value to the total functional value in the ASAU was calculated. For each ASAU, the calculation formula was as follows:

$$V_i = \sum_{j}^{n} N_j \times S_j \tag{2}$$

$$R_i = \frac{V_i}{\sum_{i=1}^{4} V_i} \tag{3}$$

where V_i is the functional value of the i-th type of PLES within the ASAU, R_i is the ratio of the V_i within the ASAU, N_j is the total number of the j-th type of POI data, and S_j is the final score of the j-th type of POI data. When the R_i within the ASAU is higher than 50%, the ASAU is identified as the corresponding i-th type of PLES. While the ratios of all types of R_i within the ASAU are lower than 50%, the ASAU is identified as a mixed space, and further identification is carried out manually based on remote sensing images and POI data.

Due to the limitation of POI data, the ASAUs that do not contain any POI remain unidentified even after the previous two steps. After the investigation of these ASAUs based on POI data, RSIs, and LC data, two main types of this phenomenon were observed, including rural settlements (Figure 3a) and large industrial bases (Figure 3b). Due to the high cost of POI data collection, generation, and maintenance and the low intensity of economic activities within rural settlements, data providers may be reluctant to invest resources in rural settlements to collect and update POI data. For some large industrial bases with large physical footprints, such as steel plants, their representation in POI data is one or a few points. From the SAU perspective, POIs that represent large industrial bases may appear in only one or a few of the multiple SAUs that actually contain large industrial bases.

Based on this investigation, we drew inspiration from Voxel-Based Region Growing (VBRG) in point cloud segmentation algorithms [51] to establish a simple rule for differentiating NAPS and LS in the ASAU without POI distribution. The illustrative diagram of the rule is shown in Figure 4, and the detailed steps are as follows:

Step 1: The SAUs identified as NAPS and adjacent to the SAUs identified as AS were selected as the initial seed SAUs.

Step 2: All the adjacent SAUs to the initial seed SAUs were traversed. If an adjacent SAU was identified as AS, it would be re-identified as NAPS and selected as a new seed SAU.

Step 3: The new seed SAUs obtained in Step 2 were treated as the initial seed SAUs for the next iteration.

Step 4: Repeat steps 2 and 3 until no new seed SAUs are generated.

Step 5: Stop traversing, and the remaining SAUs that were still identified as AS were reidentified as LS.

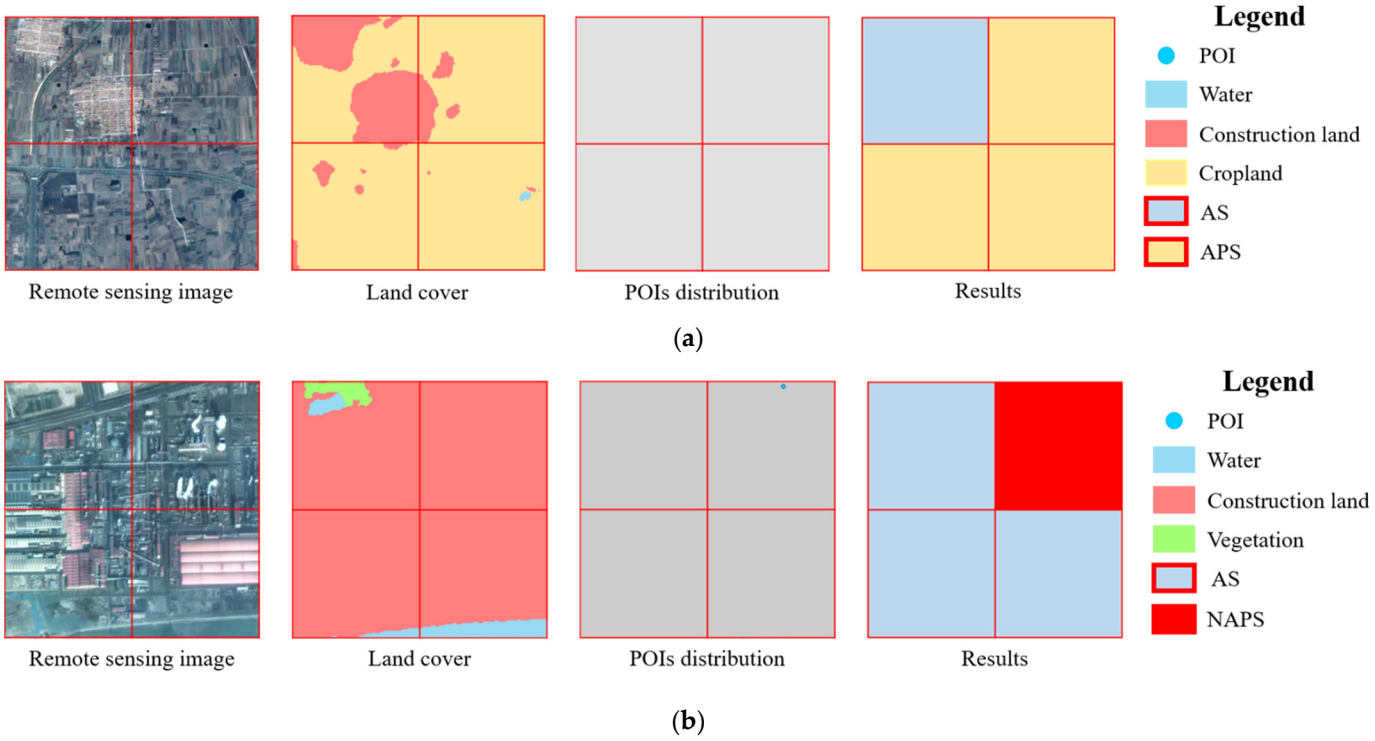

Figure 3. Two main scenarios that cause the lack of POI distribution in a portion of AS. (**a**) Rural settlement; (**b**) Large industrial base.

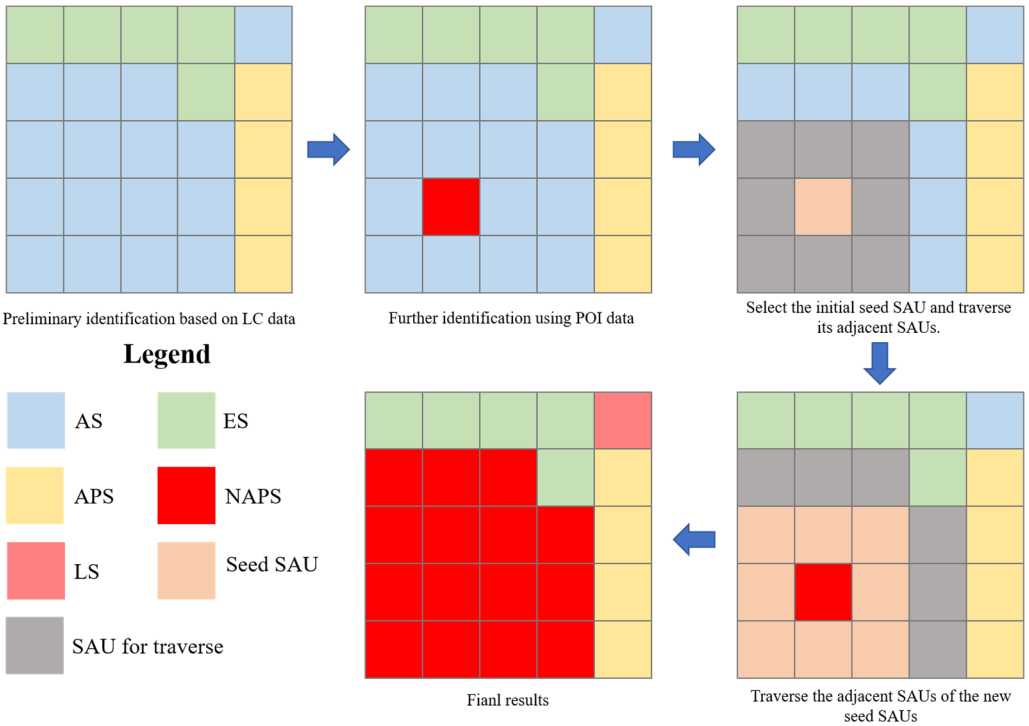

Figure 4. Illustrative diagram of differentiating LS and NAPS in the AS without POI distribution.

2.5. Methods for Characterizing the Characteristics of PLES and PLES Change

2.5.1. Kernel Density Estimation

Kernel Density Estimation (KDE) is a nonparametric statistical method that can explore the distribution of data without a priori assumptions and has been widely used in spatial

pattern analysis, criminal geography, and other studies [52]. In this study, the area of each SAU was used as a weight to avoid biased results due to the neglect of significant differences in the area of different SAUs. The calculation formula is as follows:

$$f(s) = \frac{1}{nh^2}\sum_{i=1}^{n} K\left(\frac{w_i \times d(s, x_i)}{h}\right) \quad (4)$$

where n is the number of SAU, h refers to the bandwidth set artificially, $K()$ refers to the kernel function selected artificially, and $d(s, x_i)$ refers to the distance from the steel plant i to the location s.

KDE requires the manual setting of two parameters: the kernel function K and the bandwidth h. The choice of kernel function has little effect on the results; however, the choice of bandwidth has a great impact on the results [53]. In this study, we refer to the literature [50] for the dynamic selection of bandwidth according to the characteristics of the data.

2.5.2. Land Use Transfer Matrix for PLES

As the most widely used method in land use/cover change (LUCC)-related studies, the land use transfer matrix is able to comprehensively and specifically reflect the changes in land use structure [54]. The single land use dynamic degree is able to quantitatively represent the drastic degree of land use change over a period of time, which plays an important role in land use-related research [55]. In this study, spatial overlay analysis was used to obtain the changing regions of PLES. Based on the changing regions of PLES, the area of PLES change and Single PLES Dynamic Degree (SPLESDD) were calculated for constructing the PLES Transfer Matrix (PLESTM). The form of PLESTM is shown as follows:

$$PLESTM = \begin{bmatrix} PLES_{11} & \cdots & PLES_{1n} & SPLESDD_1 \\ \vdots & \ddots & \vdots & \vdots \\ PLES_{n1} & \cdots & PLES_{nn} & SPLESDD_n \end{bmatrix}, n = 4 \quad (5)$$

where n is the number of PLES types, $PLES_{ij}$ refers to the area converted from PLES type i to PLES type j, and $SPLESDD_i$ refers to the SPLESDD of PLES type i, which can be calculated by Formula (6).

$$SPLESDD_i = \frac{PLES(i, t_2) - PLES(i, t_1)}{\Delta t \times PLES(i, t_1)} \times 100\% \quad (6)$$

where $SPLESDD_i$ refers to the SPLESDD of the PLES type i, $PLES(i, t_1)$ and $PLES(i,t_2)$ respectively refer to the area of PLES type i for the start year t_1 and the end year t_2, $\Delta t = t_2 - t_1$.

2.5.3. Spatial Autocorrelation Analysis

Spatial autocorrelation analysis is able to quantitatively characterize the degree of spatial correlation of one or more geographic variables and is widely used in PLES-related studies [5,29,56]. In this study, Moran's I and bivariate Moran's I were used to explore the spatial correlation of PLES. The calculated results fall within the range of $[-1, 1]$. After passing the significance test, a positive calculated result indicates that the variables are spatially positively correlated, while a negative calculated result indicates that the variables are spatially negatively correlated. The larger the absolute value of the calculated result, the stronger the correlation. When the calculation result equals 0, the variables have no spatial correlation; that is, the spatial distribution is random. The calculations of Moran's I and bivariate Moran's I were carried out using Geoda version 1.20.

3. Results

3.1. Results of PLES Identification

3.1.1. Results of UBUA Extraction and SAU Division

The UBUA of Jiaodong Peninsula in 2022 was extracted using POI data and LC data. As shown in Table 4, the actual UBUA area (marked as ground truth) disclosed in the statistical yearbook was used to evaluate the effect of the UBUA extraction results, including the results using solely the Densi-Graph method (marked as initial results) and the results using LC data to optimize the UBUA boundaries of the initial results (marked as final results). As can be seen from Table 4, the differences between the areas of the initial results and the corresponding ground truth were significant, while the differences between the areas of the final results and the corresponding ground truth were relatively reduced.

Table 4. The difference between the area of UBUA extraction results and ground truth.

	Ground Truth [1]	**POI (Difference)** [2]	**POI + LC (Difference)** [3]
Qingdao City	964.39 km^2	1096.94 km^2 (+13.74%)	932.69 km^2 (−3.29%)
Yantai City	629.52 km^2	707.57 km^2 (+12.40%)	593.86 km^2 (−5.66%)
Weihai City	293.02 km^2	322.69 km^2 (+10.13%)	289.99 km^2 (−1.03%)

[1] The ground truth was obtained from the urban construction statistical yearbook. [2] The POI refers to the initial UBUA extraction results using the Densi-Graph method with POI data. [3] The POI + LC refers to the final UBUA extraction results using land cover data to optimize the boundaries of the initial results.

The UBUA extraction results and the zoomed-in views of the verification areas are shown in Figure 5. As can be seen from Figure 5a, the final UBUA extraction results were basically consistent with the continuous construction land; however, a portion of the continuous construction land was overlooked. In addition, several UBUAs with relatively small areas appeared in the final UBUA extraction results. Three areas marked as area I, II, and III were selected for local verification. According to Figure 5b,c, the final UBUA extraction results provided more detailed boundary representations than the initial results. According to Figure 5d,e, the area II represents an industrial zone located on the edge of the UBUA. Compared with the urban central area, the POI distribution in this area was sparse, which resulted in a relatively low KDE value. According to Figure 5f,g, area III was close to the main UBUA, which may be the result of the outward UBUA expansion. Area III mainly consists of residential areas with a dense distribution of POIs and a relatively high KDE value. From the perspective of the UBUA definition, the results for areas II and III were correct. Overall, the quality of the UBUA extraction results is high and sufficient to support subsequent research endeavors.

Based on the UBUA extraction results for 2022, the blocks segmented by road network data in 2018 and 2022, as well as 1 km × 1 km regular geographic grids, were used for the SAU construction. As a result, the number of UBUA SAUs in 2018 was 10,156, and that in 2022 was 10,341. For NUBUA SAUs, the number was 31,324 both in 2018 and 2022.

3.1.2. Results of PLES Identification

In order to evaluate the quality of identification results, a verification SAU set was constructed based on the SAUs selected by regular grid points and random points. Firstly, the regular grid points were constructed at 10 km intervals, and the SAUs intersecting with the regular grid points were selected to join the verification SAU set. Since most of the regular grid points were located in the NUBUA, 100 random points within the UBUA were constructed, and the SAUs intersecting with the random points were selected to join the verification SAU set. The verification result showed that the accuracy was 87.90% (356/405). It should be noted that the PLES identification results for verification were selected from the PLES identification results in 2022. The identification results of PLES and the spatial distribution of the verification SAUs are shown in Figure 6.

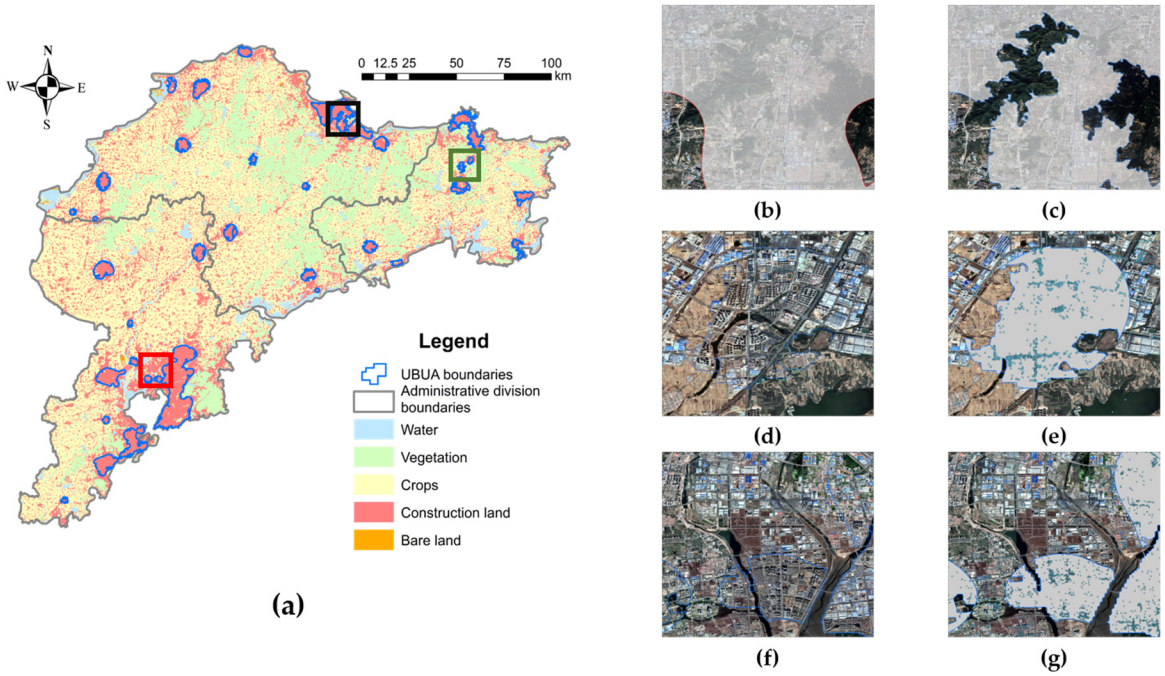

Figure 5. Extraction results of UBUA and zoomed-in views of verification areas. (**a**) The final UBUA extraction results, where the black box refers to the location of the verification area I, the green box refers to the location of the verification area II, and the red box refers to the location of the verification area III; (**b**) The initial UBUA extraction results in the verification area I; (**c**) The final UBUA extraction results in the verification area I; (**d**) Remote sensing images of the verification area II; (**e**) POI distribution of the verification area II; (**f**) Remote sensing images of the verification area III; (**g**) POI distribution of the verification area III.

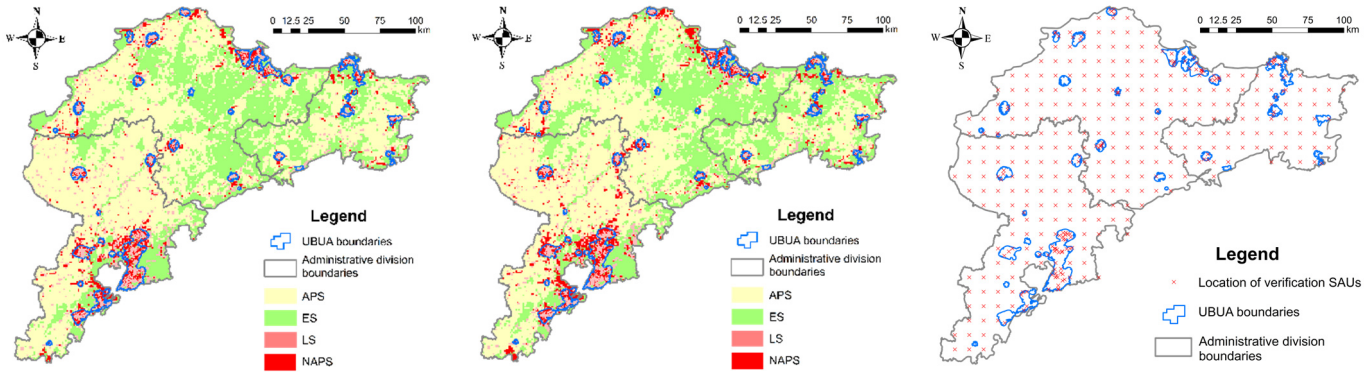

Figure 6. Identification results of PLES and spatial distribution of verification SAUs. (**a**) Identification results of PLES in 2018; (**b**) Identification results of PLES in 2022; (**c**) Illustrative diagram of the spatial distribution of the verification SAUs.

3.2. Spatial Pattern Characteristics of PLES in Jiaodong Peninsula

The KDE results of the different types of PLES identification results are shown in Figure 7. In terms of spatial distribution, APS and ES were the main PLES types in the Jiaodong Peninsula. The high-density areas of APS were distributed in eastern and western Jiaodong Peninsula, with a more extensive distribution observed in the western part. While the high-density areas of ES were distributed in the center of the Jiaodong Peninsula. The spatial distribution of LS and NAPS was more concentrated, mainly in the coastal areas.

For LS, the high-density areas were distributed in the southern coastal area of Qingdao City, northeastern coastal area of Yantai City, and the northern coastal area of Weihai City. For NAPS, the high-density areas were distributed in the southern coastal area of Qingdao City and the northeastern coastal area of Yantai City. In addition, a significant differentiation between UBUA and NUBUA was shown in the spatial distribution of PLES on the Jiaodong Peninsula. The high-density areas of LS were mainly distributed within the UBUA, and the high-density areas of NAPS were mainly distributed nearby the UBUA boundaries, while several high-density distributions of NAPS within the UBUA were observed. On the contrary, the high-density areas of APS and ES were mainly distributed within NUBUA.

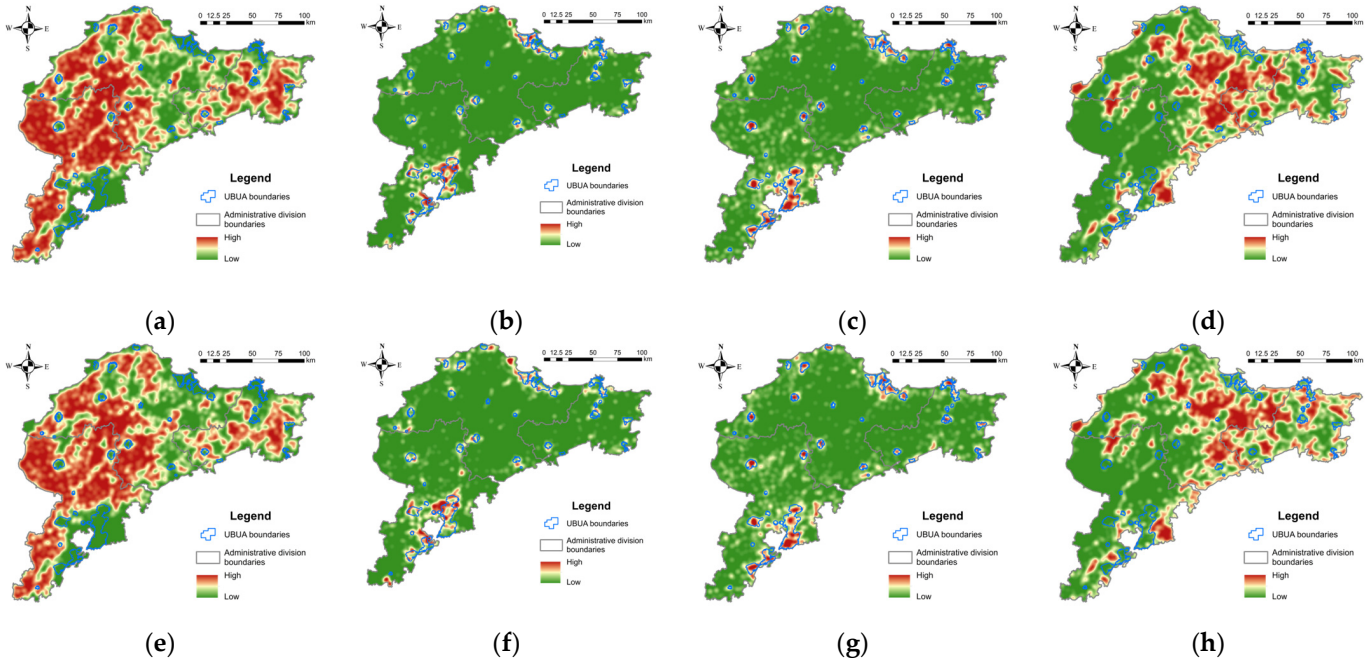

Figure 7. KDE results of PLES. (**a**) KDE results of APS in 2018; (**b**) KDE results of NAPS in 2018; (**c**) KDE results of LS in 2018; (**d**) KDE results of ES in 2018; (**e**) KDE results of APS in 2022; (**f**) KDE results of NAPS in 2022; (**g**) KDE results of LS in 2022; (**h**) KDE results of ES in 2022.

The queen adjacency method based on the spatial adjacent relation was selected to construct the spatial weight matrices for spatial autocorrelation analysis. The SAUs adjacent to the independent variable were treated as dependent variables. In addition to the computation of all SAUs within the Jiaodong Peninsula, SAUs within the UBUA and the NUBUA were computed separately. The calculation results are shown in Table 5. The results on the diagonal line in the table refer to the results of Moran's I, and the other elements refer to the results of bivariate Moran's I, which are the same below.

From the calculation results, it can be seen that all the types of PLES within the Jiaodong Peninsula showed significantly positive spatial autocorrelation. Among them, the spatial autocorrelation of APS was the most significant, while the spatial autocorrelation of NAPS was weaker than that of the other three types. Regarding the spatial correlation of different types of PLES, APS showed a negative spatial correlation with the other three types of PLES. NAPS showed a positive spatial correlation with ES and a negative spatial correlation with ES. LS showed a negative spatial correlation with ES.

Within the UBUA, significantly positive spatial autocorrelation was observed in NAPS, LS, and ES, among which the spatial autocorrelation of LS and NAPS was more significant and the calculation results were closer. In contrast, the spatial autocorrelation of ES was weaker, and the calculation result decreased in 2022 compared to 2018, while there was no significant change in the other three types of PLES. In addition, NAPS showed a significantly negative spatial correlation with LS.

Table 5. Spatial autocorrelation results for the PLES.

Calculation Range		Calculation Results for 2018				Calculation Results for 2022			
		APS	**NAPS**	**LS**	**ES**	**APS**	**NAPS**	**LS**	**ES**
Jiaodong Peninsula [1]	APS	0.692	−0.210	−0.323	−0.303	0.684	−0.220	−0.300	−0.306
	NAPS		0.363	0.122	−0.142		0.396	0.115	−0.155
	LS			0.518	−0.213			0.500	−0.201
	ES				0.629				0.619
UBUA [2]	APS	0.031	−0.011	−0.096	0.018	0.032	0.020	−0.051	0.025
	NAPS		0.455	−0.410	−0.035		0.433	−0.421	−0.020
	LS			0.457	−0.086			0.436	−0.042
	ES				0.253				0.158
NUBUA [3]	APS	0.603	−0.096	−0.056	−0.559	0.597	−0.117	−0.068	−0.530
	NAPS		0.355	0.107	−0.087		0.361	0.101	−0.094
	LS			0.190	−0.073			0.195	−0.070
	ES				0.646				0.624

[1] The Jiaodong Peninsula refers to the results calculated using all SAUs on the Jiaodong Peninsula. [2] The UBUA refers to the results calculated using the specific SAUs located within the UBUA in the Jiaodong Peninsula. [3] The NUBUA refer to the results calculated using the specific SAUs located within the NUBUA on the Jiaodong Peninsula.

The spatial relationships of the PLES showed different patterns within the NUBUA. APS, NAPS, and ES within the NUBUA showed significantly positive spatial autocorrelation, among which the spatial autocorrelation of APS and ES was the most significant. LS, on the other hand, showed weak spatial autocorrelation, which was significantly weaker than that within the UBUA. LS and NAPS showed a positive spatial correlation within the NUBUA, whereas within the UBUA, the spatial correlation was significantly negative. The calculation result of ES within the NUBUA also decreased in 2022; however, the decrease was weaker than that in the UBUA.

3.3. Spatio-Temporal Changes in PLES in Jiaodong Peninsula during 2018–2022

Based on the spatial overlay analysis, the change areas of PLES in the Jiaodong Peninsula during 2018–2022 were obtained from the PLES identification results for 2018 and 2022. Based on the change areas of PLES, PLESTM was calculated. The calculation results are shown in Table 6. For the convenience of description, A-B is used in the following text to represent the conversion from PLES type A to PLES type B.

In terms of change area, the interconversion of APS and ES was relatively drastic in the Jiaodong Peninsula. In addition to the two PLES change types, the PLES change in Jiaodong Peninsula mainly manifested the increase of NAPS and LS, including APS-NAPS, APS-LS, NAPS-LS, ES-NAPS, and ES-LS. The mentioned seven types of PLES change were considered to be the main PLES change types and were further analyzed. In terms of dynamic degree, the most drastic change occurred in LS, with an increasing trend. It was followed by NAPS, which also showed an increasing trend. The changes in APS and ES were relatively more moderate, with APS showing a slight decreasing trend and ES showing a slight increasing trend.

Table 6. Calculation results of the PLESTM.

	APS (km^2)	**NAPS (km^2)**	**LS (km^2)**	**ES (km^2)**	**SLUDD (%/Year)**
APS	15,462.29	76.31	58.51	1048.36	−0.45
NAPS	9.41	1681.46	30.21	8.81	1.64
LS	3.03	12.23	2677.98	18.38	2.41
ES	853.96	73.70	111.60	9410.54	0.09

The spatial distribution of PLES change in the Jiaodong Peninsula and the KDE results of the seven main types of PLES change are shown in Figure 8. In an overall view, the spatial

distribution of the PLES change was mainly distributed in the NUBUA. In terms of the interconversion of ES and APS, ES-APS was concentrated in the central Jiaodong Peninsula, while APS-ES was mainly distributed in the eastern and northeastern Jiaodong Peninsulas. The increase in LS, including APS-LS, NAPS-LS, and ES-LS, was mainly distributed in the southwestern coastal area of the Jiaodong Peninsula, specifically in the southern coastal area of Qingdao City. In addition, ES-LS also occurred in the southern coastal area of Weihai City. Among them, APS-LS and ES-LS are mainly distributed around the UBUA, while NAPS-LS is mainly distributed inside the UBUA. The distribution in the increase of NAPS was more scattered, with ES-NAPS mainly distributed in the northern Jiaodong Peninsula, specifically in the northern Yantai City, while APS-NAPS was mainly distributed in the eastern Qingdao City.

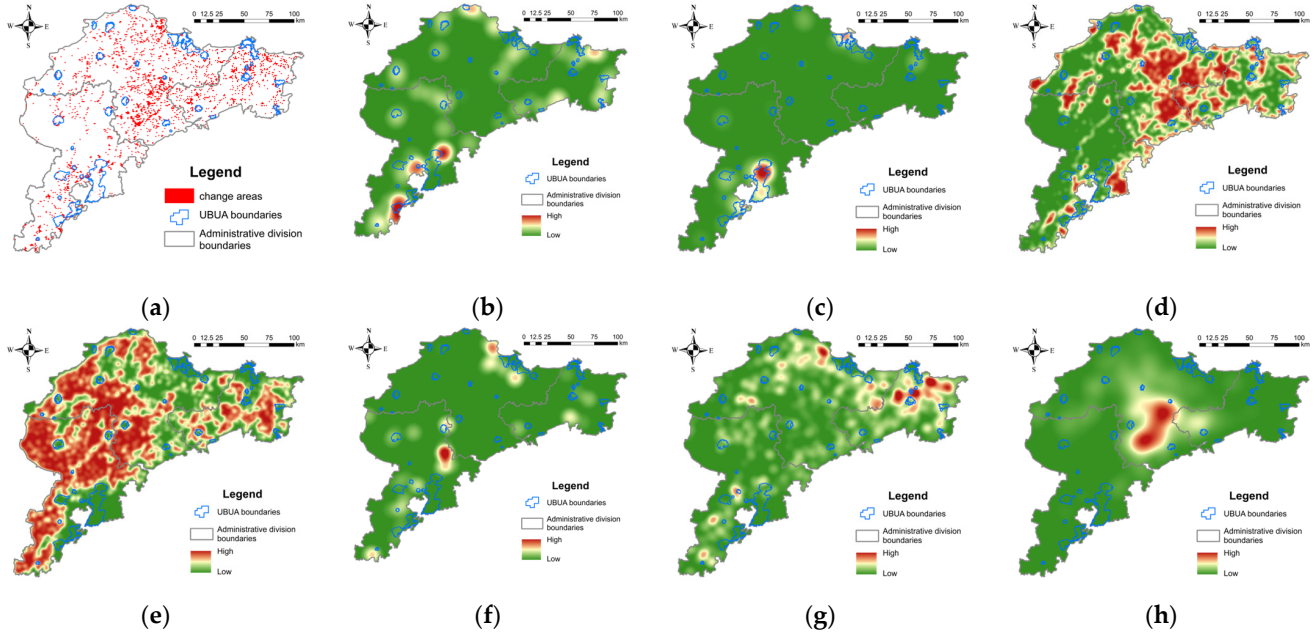

Figure 8. Spatial distribution of PLES change and KDE results of the main types of PLES change. (**a**) Spatial distribution of the PLES change; (**b**) KDE results of APS-LS; (**c**) KDE results of NAPS-LS; (**d**) KDE results of ES-LS; (**e**) KDE results of ES-NAPS; (**f**) KDE results of APS-NAPS; (**g**) KDE results of APS-ES; (**h**) KDE results of ES-APS.

Considering that the changing SAUs were not necessarily adjacent, the distance-based method was selected to construct the spatial weight matrixes. The SAUs within 5 km of the independent variable SAUs were treated as the dependent variable SAUs. The calculation results are shown in Table 7. According to the results, APS-ES and ES-APS showed significantly positive spatial autocorrelation, while some degree of positive spatial autocorrelation was shown in ES-LS and ES-APS. Additionally, APS-ES demonstrated a relatively strong negative spatial correlation with ES-APS and ES-LS.

Table 7. Spatial autocorrelation results for the PLES change.

	APS-LS	**APS-NAPS**	**APS-ES**	**NAPS-LS**	**ES-LS**	**ES-APS**	**ES-NAPS**
APS-LS	−0.003	0.031	−0.019	0.052	−0.007	0.019	−0.007
APS-NAPS		0.084	−0.036	0.043	0.018	0.013	0.003
APS-ES			0.619	−0.014	−0.049	−0.280	−0.059
NAPS-LS				0.052	0.037	−0.026	−0.010
ES-LS					0.132	−0.003	−0.001
ES-APS						0.509	−0.405
ES-NAPS							0.168

4. Discussion

4.1. Visual Comparison forPLES Change

In order to further evaluate the LPES identification results and explore the real-world situation and the driving mechanism of the PLES change in Jiaodong Peninsula, eight typical areas were selected as verification areas based on the seven main types of PLES change for visual comparison. Among them, two areas were selected for the verification of APS-ES, respectively marked as verification area A and verification area B. The spatial distribution of the verification areas is shown in Figure 9.

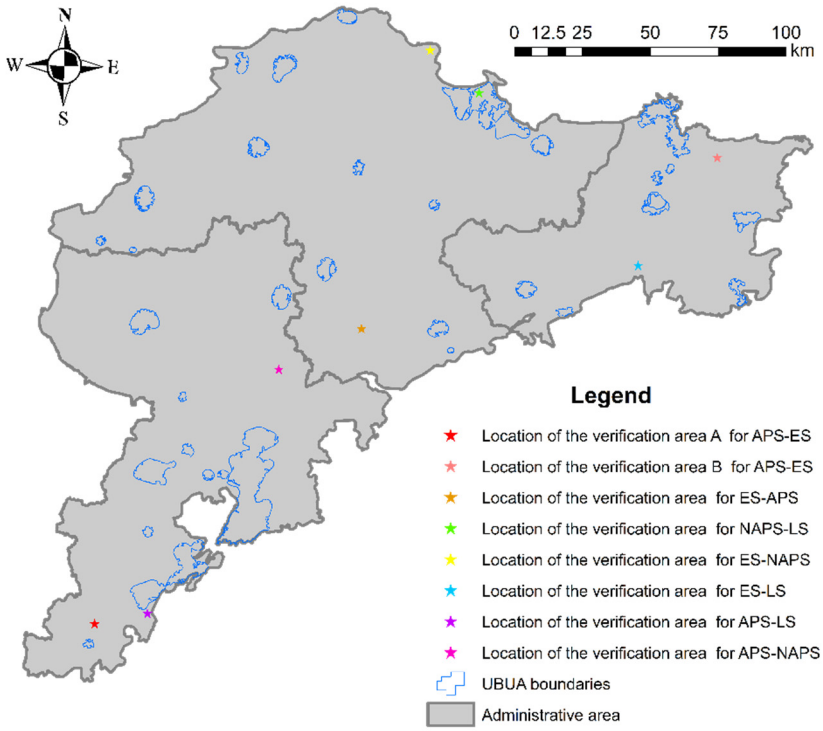

Figure 9. Spatial distribution of the verification areas.

The dramatic interconversion of ES and APS first caught our attention. Among them, the ES-APS was mainly distributed in southern Yantai City, which was planned as a grain-producing area in the "Territorial spatial planning of Yantai City (2021–2035)". Driven by economic interests, many farmers use arable land originally intended for grain cultivation to grow fruit trees or other cash crops, known as non-grain production in agricultural land (NGPAL) [57]. The Chinese government discourages such practices due to the enormous demand for food and the limited availability of arable land resources. In 2020, the State Council issued the "Opinions on preventing non-grain production of cultivated land and stabilizing food production", which required the governments at all levels in China to strengthen incentives and constraints as well as enhance supervision of NGPAL. In this context, the Yantai municipal government implemented a series of incentives and penalties, increased the subsidies for grain cultivation, and strengthened the supervision of NGPAL. Cultivated land that had been used to grow other cash crops was replanted with grain (Figure 10(a1–a4)). Furthermore, the re-cultivation of abandoned cultivated land may also be a potential reason for the ES-APS. Factors such as climate variations, declining cultivation conditions, and rural labor migration can lead to the emergence of abandoned cultivated land [58]. Prolonged abandonment of cultivated land may result in the overgrowth of weeds and a decline in soil fertility. With increasing attention to food security, the government has paid more attention to addressing this issue in recent years [59]. Subsidy policies, active construction of agricultural facilities, and the recovery and re-allocation of abandoned cultivated land were among the measures employed by

government authorities to avoid the waste of cultivated land resources, leading to the restoration of many previously abandoned cultivated lands. However, it should be noted that due to the lack of field surveys, this study cannot draw detailed conclusions in this regard.

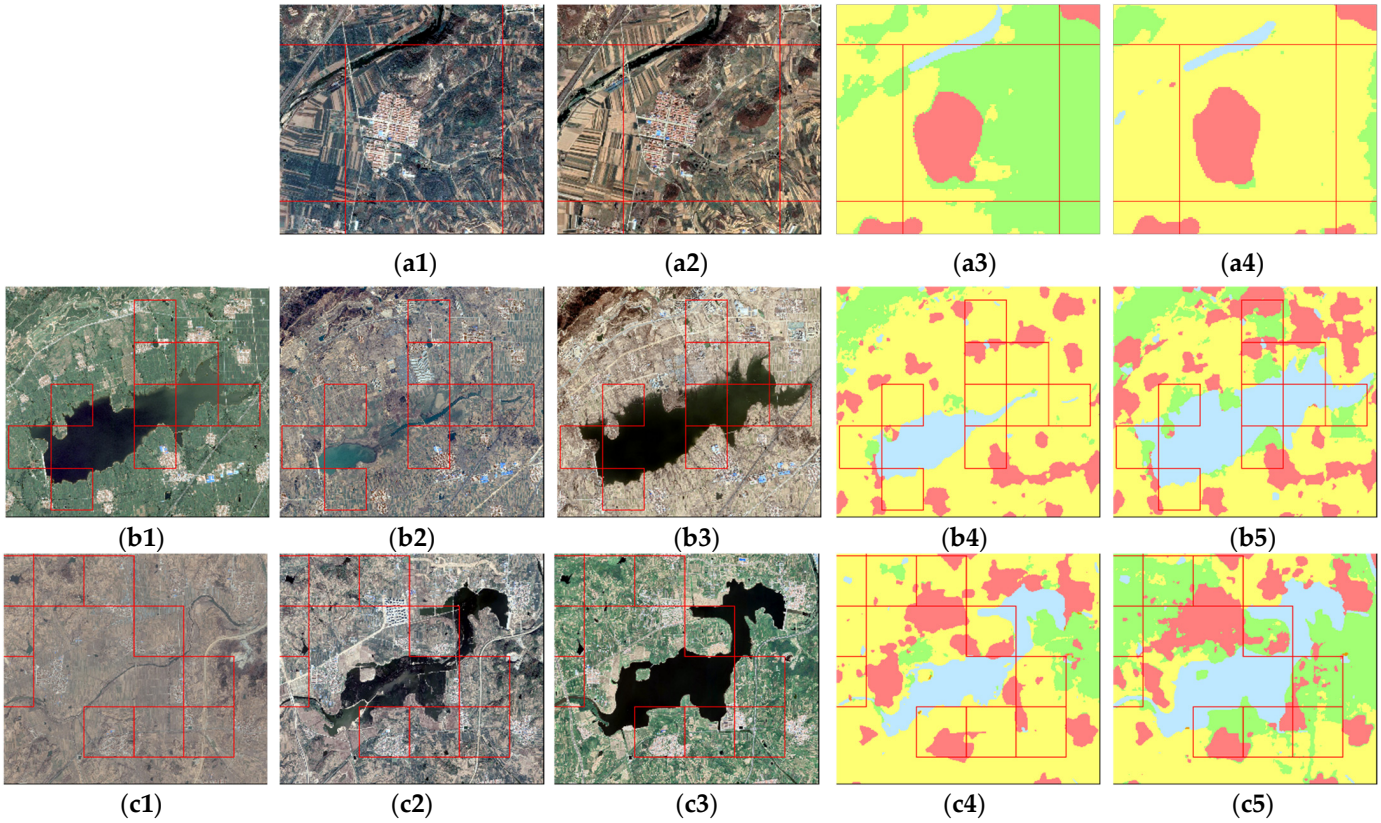

Figure 10. Visual comparisons for ES-APS and APS-ES, where the red boxes represent the area within which corresponding changes occur. The legend for land cover data is the same as in Figure 4, where red represents construction land, yellow represents crops, blue represents water, and green represents vegetation. (**a1**) RSI of the ES-APS verification area in 2018; (**a2**) RSI of the ES-APS verification area in 2022; (**a3**) LC of the ES-APS verification area in 2018; (**a4**) LC of the ES-APS verification area in 2022; (**b1**) RSI of the verification area A of APS-ES in 2014; (**b2**) RSI of the verification area A of APS-ES in 2018; (**b3**) RSI of the verification area A of APS-ES in 2022; (**b4**) LC of the verification area A of APS-ES in 2018; (**b5**) LC of the verification area A of APS-ES in 2022; (**c1**) RSI of the verification area B of APS-ES in 2014; (**c2**) RSI of the verification area B of APS-ES in 2018; (**c3**) RSI of the verification area B of APS-ES in 2022; (**c4**) LC of the verification area B of APS-ES in 2018; (**c5**) LC of the verification area B of APS-ES in 2022.

The changes in the water had a significant effect on APS-ES, and the effect could be divided into two scenarios. As shown in Figure 10(b1–b5), the first scenario was the effect of the storage of reservoirs, reflected in validation area A, which is located at the Douyazi Reservoir in Qingdao City. According to the "Qingdao water resources statistical bulletin" published by the Qingdao Municipal Water Administration Bureau, rainfall in Qingdao City was continuously low from 2013 to 2017 with no effective runoff formation. The surface water and the groundwater were not effectively replenished, resulting in a serious shortage of the water storage in the reservoirs in 2018. Due to the prolonged lack of water, the villagers around the reservoirs reclaimed the farmland for cultivation on the sides of the reservoirs. The rainfall in Qingdao City from 2020 to 2021 significantly increased, and the water storage in the reservoirs consequently increased. The total amount of reservoir water

storage in Qingdao was 430.1 million cubic meters in 2021, which represents an increase of 110.94% compared to 203.9 million cubic meters in 2017.

As shown in Figure 10(c1–c5), the different scenario was the occupation of cultivated land by the new reservoir construction, reflected at the validation area B, which is located the Poyu Reservoir in Weihai City. The economic and social development of the Jiaodong Peninsula constrained by the scarcity of freshwater resources for a long time. The water resources needed for industrial production and residential life on the Jiaodong Peninsula had long relied on the Jiaodong Water Diversion Project. The transferred water temporarily solved the shortage of water in the Jiaodong Peninsula; however, in the face of increasing demand for freshwater resources, it is impractical to rely solely on expensive and restrictive transferred water. Faced with the dilemma of a freshwater shortage, the cities located on the Jiaodong all introduced corresponding modern water network construction plans. To reduce the excessive reliance on transferred water and enhance urban emergency water supply capabilities, key water storage construction, including the construction of new reservoirs, expansion of existing reservoirs, and strengthening regional water system connections, was mentioned in the plans.

The increase in LS, including APS-LS, NAPS-LS, and ES-LS, was mainly distributed within the UBUA or around the UBUA boundary. Due to the rapid socio-economic development and urbanization of the Jiaodong Peninsula, many populations have flocked to the UBUA. With the increase in population, more residential land and infrastructure are needed to meet people's living needs, which inevitably leads to the expansion of LS. Due to the well-developed infrastructure within the existing UBUA, expanding at the existing UBUA boundary allows for better utilization of the already established facilities and public services, such as transportation, water supply, and drainage systems, thereby reducing the cost of constructing new infrastructure. However, the expansion pattern may also result in the occupation of cultivated land in the surrounding areas of the UBUA. The APS-LS was mainly concentrated around the boundaries of the UBUA (Figure 11(a1,a2)).

Urban development with unlimited outward expansion may lead to a series of urban problems, such as the heat island effect, traffic congestion, and environmental pollution [60]. Satellite city development patterns are an important approach to alleviating population pressure in urban centers and preventing further deterioration of urban issues [61]. The increase in LS away from the existing UBUA was observed in the Nanhai New District, located in the southern coastal area of Weihai City (Figure 11(b1,b2)). As a key development area of the Shandong Blue Economic Zone, the Nanhai New District has developed rapidly and serves as a crucial strategic node for the southward development of Weihai City. A newly planned university town was located in the verification area. The construction of the university town can deliver talents for the development of the port industry in Nanhai New District. While the spillover effects will stimulate economic growth and infrastructure improvement in the surrounding areas, promoting the urbanization process and further alleviating the population pressure in the urban center [62–64].

NAPS-LS was mainly the conversion of industrial land to residential land, concentrated within the UBUA (Figure 11(c1,c2)). This phenomenon reveals another pattern of UBUA development, namely urban renewal. As the inefficiency of land use in the process of urbanization has become apparent, "increment expansion", which is mainly based on increasing the built-up area, has gradually changed to "inventory optimization", namely, optimizing the functional layout of the city and tapping into the inventory of land without increasing the built-up area, in order to ease the contradiction between people and land and to achieve economic growth [65]. NAPS-LS within the UBUA could alleviate urban population pressure on the one hand and reduce the impact of industry on the human settlement environment inside the UBUA on the other. In addition, the relocation and reorganization of industrial parks can have positive impacts on enterprises to eliminate backward equipment and promote industrial upgrading. It should be noted that, due to the untimely update of POI data, some of the dismantled industrial parks were still identified as NAPS in the identification results for 2022.

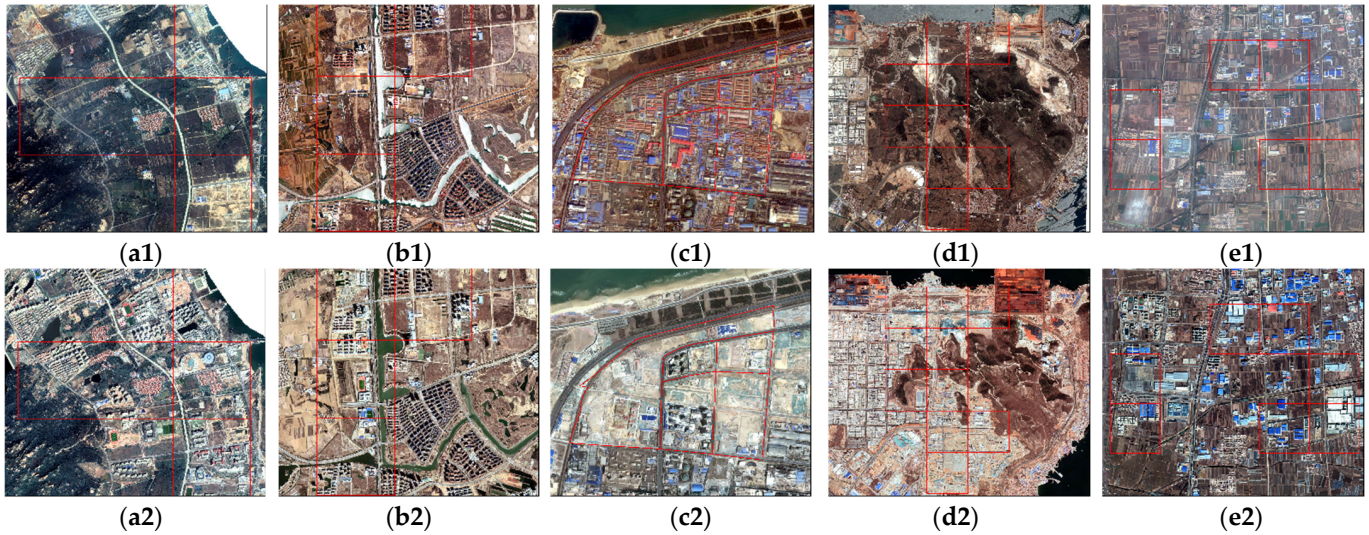

Figure 11. Visual comparisons for APS-LS, ES-LS, NAPS-LS, ES-NAPS, and APS-NAPS, where the red boxes represent the area within which corresponding changes occur. (**a1**) RSI of the APS-LS verification area in 2018; (**a2**) RSI of the APS-LS verification area in 2022; (**b1**) RSI of the ES-LS verification area in 2018; (**b2**) RSI of the ES-LS verification area in 2022; (**c1**) RSI of the NAPS-LS verification area in 2018; (**c2**) RSI of the NAPS-LS verification area in 2022; (**d1**) RSI of the ES-NAPS verification area in 2018; (**d2**) RSI of the ES-NAPS verification area in 2022; (**e1**) RSI of the APS-NAPS verification area in 2018; (**e2**) RSI of the APS-NAPS verification area in 2022.

The main sources of NAPS increases were APS and ES. The spatial distribution of ES-NAPS was mainly located in the coastal area (Figure 11(d1,d2)). The Jiaodong Peninsula is surrounded by the sea on three sides, offering abundant marine resources and favorable port conditions. The validation area is located in the west port area of Yantai Port, which was the core planned and developed port area of Yantai Port. Unlike the existing core port area of Yantai Port, which is adjacent to the main urban area, the west port area lacked large and mature urban residential areas, making it suitable for the development of heavy industries. Additionally, the transportation conditions in the west port area were convenient, facilitating the construction of a logistics park in the vicinity. Promoting the construction of the blue economy industrial zone based on port industrial parks and logistics parks can lead to the layout optimization, transformation, and upgrading of regional heavy industry. The construction and development of the west port area are of great significance to the transformation and upgrading of Yantai Port and the implementation of the strategy of consolidating to the east and developing to the west in Yantai City.

The APS-NAPS was mainly distributed in western Qingdao City at the border with Yantai City (Figure 11(e1,e2)). The validation area is located in the new energy automobile industry agglomeration area of Jiangshan Town, which is located in the geometric center of Qingdao City, Yantai City, Weihai City, and Weifang City and offers obvious location advantages. As the core area of the national urban-rural integration development pilot zone and one of the four functional strategic node towns of Qingdao City, Jiangshan Town actively attracts investment and promotes industrial agglomeration. In July 2020, the manufacturing plant headquarter of Beijing Automotive Industry Holding Co., Ltd. (BAIC) relocated to Jiangshan Town, attracting upstream and downstream supporting industries to aggregate in Jiangshan Town, forming a relatively complete new energy vehicle industry chain including new energy vehicle components, electric motors, electric batteries, vehicle production, and automotive aftermarket.

4.2. Discussion and Policy Implications Based on the Results and the Real-World Situation

The continuous change of the urban underlying surface towards impermeable surfaces is a distinctive feature of the urbanization process, which may lead to several urban

issues [66]. On the one hand, during heavy rainfall, the impermeable surfaces prevent rainwater from effectively infiltrating the ground, causing urban areas to be unable to discharge excess water in a short period, of time leading to urban floods or waterlogging. On the other hand, impermeable surfaces have a higher heat absorption rate and a lower specific heat capacity compared to other underlying surfaces. They continuously absorb radiation and release heat into their surroundings, contributing to the urban heat island effect. The Jiaodong Peninsula is currently facing the issue of the urban heat island effect [67]. Flood disasters and the urban heat island effect are issues that urban policymakers must consider, which could potentially pose threats to urban economic development and residents' health. To enhance urban resilience and improve the city's ability to withstand flood disasters, the Chinese government has proposed the concept of constructing sponge cities. The vision of the sponge city is to make cities act like sponges, absorbing, storing, infiltrating, and purifying rainwater, and then releasing and utilizing the stored water when needed. The construction of sponge cities not only effectively enhances the city's ability to resist flooding but also provides a solution to the water scarcity problem on the Jiaodong Peninsula through positive stormwater management [68]. Furthermore, the construction of sponge cities and the alleviation of the urban heat island effect are compatible in various aspects, including technology, finance, institutional, and social aspects, and have co-benefits [69]. The compatibility of water scarcity and urban heat island mitigation measures could be considered when planning for sponge city construction.

At present, ensuring food security and realizing self-sufficiency in food are important issues facing China. Ensuring food security is a complex, systematic project involving multiple aspects of population, land, technology, and management [70]. Cultivated land protection is the primary issue facing the realization of this goal. Urban expansion inevitably leads to the occupation of cultivated land, which is the primary problem facing cultivated land protection. Urban renewal undoubtedly provides a new idea to solve this problem by renovating old facilities within the city and optimizing the functional layout to meet the future development needs of the city [65]. For example, some old factories within UBUA can be demolished and rebuilt into residential buildings, shopping malls, or leisure service complexes to alleviate the population pressure as well as meet the growing needs of residents for a better life. The authorities in Jiaodong Peninsula had begun to try to renew the UBUA internally rather than expanding outward to meet the future development needs of the city, and this renewal is mainly reflected in the transformation of industrial land into residential land. However, no increase in ES within the UBUA was observed in our results. As mentioned before, the construction of the sponge city can provide an outstanding opportunity for Jiaodong Peninsula to solve the water shortage problem and alleviate the heat island effect. Existing studies confirmed the excellent performance of blue and green spaces (included within ES in this study) in sponge city construction [71], replenishing freshwater resource supply [72], and mitigating the heat island effect [73]. In the subsequent urban renewal process, the authorities can strengthen their consideration of the development and layout of blue and green spaces within UBUA.

In addition to the loss of cultivated land, the issue of NGP and the loss of the rural labor force can also have a strong impact on food security. Driven by economic interests, many farmers use arable land originally intended for grain cultivation to grow fruit trees or even open fishponds and plant nurseries, which seriously destroy the cultivated layer of the land [57]. In addition, policymakers have long been more concerned with planning and development within urban areas and less concerned with rural areas, which has resulted in huge gaps between urban areas and rural areas in various aspects, including residents' income and quality of life. These gaps have led to a significant influx of rural labor into urban areas, resulting in the emergence of problems such as the decline in the utilization and even abandonment of cultivated land [74]. Fortunately, these issues have received the attention of policymakers. In terms of curbing the NGPAL phenomenon, the issuance of "Opinions on preventing non-grain production of cultivated land and stabilizing food production" has given impetus to the governments at all levels in China to take action in

formulating preferential policies for grain cultivation and in the supervision of the NGPAL phenomenon in cultivated land. Regarding rural planning and construction, China has put forward the "Rural revitalization strategy", outlining a vision of a beautiful countryside with strong agriculture, picturesque rural areas, and prosperous farmers.

Improving the incomes and well-being of farmers is key to avoiding the abandonment of cultivated land and the loss of rural labor. Agricultural modernization and industrialization are helpful to increase agricultural productivity and improve the incomes and living standards of farmers [75]. However, fragmentation of cultivated land is a common phenomenon in rural China, which hinders agricultural industrialization and modernization [76]. The relatively dispersed distribution of rural settlements is a driving factor in cultivated land fragmentation and a reflection of the lack of attention paid to rural areas in land planning. Similar issues were observed in the Jiaodong Peninsula through spatial autocorrelation analysis, where the spatial autocorrelation of LS in NUBUA was significantly weaker than that in UBUA. Rural homestead is the manifestation of living space in rural China. In recent years, based on the theory of "smart shrinkage", China has implemented extensive practices in the spatial reorganization of rural homesteads, primarily through merging villages [77]. A rural homestead agglomeration through consolidation can promote the intensive use of rural land, reduce the degree of fragmentation of arable land, and contribute to the industrialization and modernization of agriculture. In addition, the aggregation of rural homesteads is helpful to the government in unifying management and reducing the cost of rural living service facilities. It should be considered by policymakers to construct appropriate living service facilities around the aggregation areas of rural homesteads. This can enhance the well-being of farmers and alleviate the pressure in urban centers.

4.3. Advantages, Limitations and Prospects

Compared to the existing methods for spatially identifying PLES, the proposed method shows a higher level of generalizability. Specifically, in contrast to the existing methods that solely rely on RSI and LC data [13,22], the proposed method offers a finer-grained identification of PS and LS, making it effectively applicable to cities or regions with primary industries in agriculture, industry, or commercial and service sectors. Furthermore, in contrast to the existing methods that solely utilize social sensing data or combine multi-source data [5,29,34,35], the proposed method effectively addressed the issues that limit the application of POI data in NUBUA, making it not only suit UBUA with pronounced human socioeconomic activities but also demonstrate robust applicability within NUBUA.

However, several limitations still exist in this study. On the one hand, the regular geographic grids with a size of 1 km $\times$ 1 km used in NUBUA may result in some errors in detail, such as the potential difficulty in identifying smaller rural settlements. On the other hand, the proposed method only considers two scenarios when further subdividing ASAUs that do not contain any POI. However, this phenomenon might vary in other study areas. Therefore, when applying this method to other study areas, conducting the necessary investigations is essential.

Future research could focus on harnessing RSI to extract a broader range of terrestrial features beyond mere land cover. Additionally, if finer-grained results are required and conditions permit, the SAU division method mentioned in the reference [30] could be considered.

5. Conclusions

Exploring the regional changes in the Production-Living-Ecological Space (PLES) is important for regional sustainable development. Rapid and accurate identification of PLES is the basis for exploring regional changes. Based on easily accessible point-of-interest (POI) and land cover (LC) data, a PLES identification method was proposed in this study. The effectiveness of the method was verified by accuracy evaluation and visual comparison.

Based on the proposed method, the PLES in Jiaodong Peninsula for 2018 and 2022 was identified, and the changes were further analyzed. According to the results, it can be observed that the spatial distribution characteristics of PLES in the Jiaodong Peninsula were obvious and showed significant differentiation between UBUA and NUBUA. Similarly, the PLES changes also showed significant differentiation between UBUA and NUBUA.

Climatic and natural resource conditions, geographic location, macro policies, and governmental behaviors drove the spatial changes of PLES in the Jiaodong Peninsula during 2018–2022. More attention to the spatial distribution planning of rural homesteads and cultivated land, as well as the co-benefits of sponge city construction and the development and layout of blue and green spaces in the process of urban renewal, could be taken into account in the future regional development and planning of the Jiaodong Peninsula.

This study proves the feasibility and potential of combining POI data and LC data in PLES spatial identification, and the results can provide a scientific reference for the optimization of regional spatial resource allocation in the Jiaodong Peninsula.

Author Contributions: Conceptualization, M.N., W.J. and Y.Z.; methodology, M.N. and Y.Z.; software, M.N. and W.J.; validation, M.N. and Y.Z.; investigation, M.N.; writing—original draft preparation, M.N., W.J., Y.Z, C.M., Y.X. and X.H. writing—review and editing, M.N., W.J., Y.Z, C.M., Y.X. and X.H.; visualization, M.N.; supervision, Y.Z. and C.M.; funding acquisition, Y.Z. and C.M. All authors have read and agreed to the published version of the manuscript.

Funding: This research was funded by the Youth Innovation Promotion Association of the Chinese Academy of Science (No. 2021126) and the National Key R&D Program of China (No. 2022YFF0606402).

Data Availability Statement: Not applicable.

Acknowledgments: The authors thank the editors and the four anonymous reviewers for their valuable comments, which helped to improve our manuscript.

Conflicts of Interest: The authors declare no conflict of interest.

Abbreviations

Acronym	Definition
API	Application Program Interface
APS	Agricultural Production Space
AS	Ambiguous Space
ASAU	Ambiguous Spatial Analysis Unit
BAIC	Beijing Automotive Industry Holding Co., Ltd.
CNY	Chinese Yuan
EIS	Evaluation Index System
ES	Ecological Space
GDP	Gross Domestic Product
KDE	Kernel Density Estimation
LC	Land Cover
LS	Living Space
LU	Land Use
LUCC	Land Use/Cover Change
MHCS	Medical and Healthy Care Service
NAPS	Non-Agricultural Production Space
NGPAL	Non-Grain Production in Agricultural Land
NUBUA	Non-Urban Built-Up Area
OSM	Open Street Map
PLEF	Production-Living-Ecological Function
PLES	Production-Living-Ecological Space
PLESTM	Production-Living-Ecological Space Transfer Matrix
POI	Point Of Interest
PS	Production Space
RSI	Remote Sensing Image

RSS	Rating and Scoring System
SAU	Spatial Analysis Unit
SCES	Science, Culture, and Education Service
SPLESDD	Single Production-Living-Ecological Space Dynamic Degree
SS	Shopping Service
UBUA	Urban Built-Up Area
VBRG	Voxel-Based Region Growing

References

1. Liu, M.; Wei, H.; Dong, X.; Wang, X.; Zhao, B.; Zhang, Y. Integrating Land Use, Ecosystem Service, and Human Well-Being: A Systematic Review. *Sustainability* **2022**, *14*, 6926. [CrossRef]
2. Yang, Y.; Bao, W.; Liu, Y. Coupling coordination analysis of rural production-living-ecological space in the Beijing-Tianjin-Hebei region. *Ecol. Indic.* **2020**, *117*, 106512. [CrossRef]
3. Zhou, D.; Xu, J.; Lin, Z. Conflict or coordination? Assessing land use multi-functionalization using production-living-ecology analysis. *Sci. Total Environ.* **2017**, *577*, 136–147. [CrossRef]
4. Duan, Y.; Wang, H.; Huang, A.; Xu, Y.; Lu, L.; Ji, Z. Identification and spatial-temporal evolution of rural "production-living-ecological" space from the perspective of villagers' behavior-A case study of Ertai Town, Zhangjiakou City. *Land Use Policy* **2021**, *106*, 105457. [CrossRef]
5. Yang, Y.; Liu, Y.; Zhu, C.; Chen, X.; Rong, Y.; Zhang, J.; Huang, B.; Bai, L.; Chen, Q.; Su, Y.; et al. Spati al Identification and Interactive Analysis of Urban Production—Living—Ecological Spaces Using Point of Interest Data and a Two-Level Scoring Evaluation Model. *Land* **2022**, *11*, 1814. [CrossRef]
6. Li, C.; Wu, J. Land use transformation and eco-environmental effects based on production-living-ecological spatial synergy: Evidence from Shaanxi Province, China. *Environ. Sci. Pollut. Res.* **2022**, *29*, 41492–41504. [CrossRef]
7. Liang, T.; Yang, F.; Huang, D.; Luo, Y.; Wu, Y.; Wen, C. Land-Use Transformation and Landscape Ecological Risk Assessment in the Three Gorges Reservoir Region Based on the "Production–Living–Ecological Space" Perspective. *Land* **2022**, *11*, 1234. [CrossRef]
8. Ji, Z.; Liu, C.; Xu, Y.; Huang, A.; Lu, L.; Duan, Y. Identification and optimal regulation of the production-living-ecological space based on quantitative land use functions. *Trans. Chin. Soc. Agric. Eng.* **2020**, *36*, 222–231. [CrossRef]
9. Ma, X.; Li, X.; Hu, R.; Khuong, M. Delineation of "production-living-ecological" space for urban fringe based on rural multifunction evaluation. *Prog. Geogr* **2019**, *38*, 1382–1392. [CrossRef]
10. Deng, Y.; Yang, R. Influence Mechanism of Production-Living-Ecological Space Changes in the Urbanization Process of Guangdong Province, China. *Land* **2021**, *10*, 1357. [CrossRef]
11. Gao, K.; Yang, X.; Wang, Z.; Zhang, H.; Huang, C.; Zeng, X. Spatial Sustainable Development Assessment Using Fusing Multisource Data from the Perspective of Production-Living-Ecological Space Division: A Case of Greater Bay Area, China. *Remote Sens.* **2022**, *14*, 2772. [CrossRef]
12. Introduction of the LU Data Published by the Chinese Academy of Sciences. Available online: https://www.resdc.cn/DOI/DOI.aspx?DOIID=54 (accessed on 16 August 2023).
13. Tao, Y.; Wang, Q. Quantitative Recognition and Characteristic Analysis of Production-Living-Ecological Space Evolution for Five Resource-Based Cities: Zululand, Xuzhou, Lota, Surf Coast and Ruhr. *Remote Sens.* **2021**, *13*, 1563. [CrossRef]
14. Yuan, J.; Zheng, Y.; Xie, X. Discovering regions of different functions in a city using human mobility and POIs. In Proceedings of the 18th ACM SIGKDD International Conference on Knowledge Discovery and Data Mining, Beijing, China, 12–16 August 2012; pp. 186–194. [CrossRef]
15. Liu, X.; He, J.; Yao, Y.; Zhang, J.; Liang, H.; Wang, H.; Hong, Y. Classifying urban land use by integrating remote sensing and social media data. *Int. J. Geogr. Inf. Sci.* **2017**, *31*, 1675–1696. [CrossRef]
16. Andrade, R.; Alves, A.; Bento, C. POI Mining for Land Use Classification: A Case Study. *ISPRS Int. J. Geo-Inf.* **2020**, *9*, 493. [CrossRef]
17. What Is the Difference between Land Cover and Land Use? Available online: https://oceanservice.noaa.gov/facts/lclu.html (accessed on 16 August 2023).
18. Li, Y.; Zhou, Y.; Zhang, Y.; Zhong, L.; Wang, J.; Chen, J. DKDFN: Domain Knowledge-Guided deep collaborative fusion network for multimodal unitemporal remote sensing land cover classification. *ISPRS J. Photogram. Remote Sens.* **2022**, *186*, 170–189. [CrossRef]
19. Digra, M.; Dhir, R.; Sharma, N. Land use land cover classification of remote sensing images based on the deep learning approaches: A statistical analysis and review. *Arab. J. Geosci.* **2022**, *15*, 1003. [CrossRef]
20. Xue, Z.; Yu, X.; Yu, A.; Liu, B.; Zhang, P.; Wu, S. Self-Supervised Feature Learning for Multimodal Remote Sensing Image Land Cover Classification. *IEEE Trans. Geosci. Remote Sens.* **2022**, *60*, 5533815. [CrossRef]
21. Venter, Z.S.; Barton, D.N.; Chakraborty, T.; Simensen, T.; Singh, G. Global 10 m Land Use Land Cover Datasets: A Comparison of Dynamic World, World Cover and Esri Land Cover. *Remote Sens.* **2022**, *14*, 4101. [CrossRef]
22. Li, H.; Fang, C.; Xia, Y.; Liu, Z.; Wang, W. Multi-Scenario Simulation of Production-Living-Ecological Space in the Poyang Lake Area Based on Remote Sensing and RF-Markov-FLUS Model. *Remote Sens.* **2022**, *14*, 2830. [CrossRef]

23. Wang, Z.; Ma, D.; Sun, D.; Zhang, J. Identification and analysis of urban functional area in Hangzhou based on OSM and POI data. *PLoS ONE* **2021**, *16*, e0251988. [CrossRef]
24. Xie, L.; Feng, X.; Zhang, C.; Dong, Y.; Huang, J.; Liu, K. Identification of Urban Functional Areas Based on the Multimodal Deep Learning Fusion of High-Resolution Remote Sensing Images and Social Perception Data. *Buildings* **2022**, *12*, 556. [CrossRef]
25. Xu, Z.; Gao, X. A novel method for identifying the boundary of urban build-up areas with POI data. *Acta Geogr. Sin.* **2016**, *71*, 928–939. [CrossRef]
26. Zhang, J.; Yuan, X.; Lin, H. The Extraction of Urban Built-Up Areas by Integrating Night-Time Light and POI Data—A Case Study of Kunming, China. *IEEE Access* **2021**, *9*, 22417–22429. [CrossRef]
27. Rosina, K.; Batista e Silva, F.; Vizcaino, P.; Herrera, M.M.; Freire, S.; Schiavina, M. Increasing the detail of European land use/cover data by combining heterogeneous data sets. *Int. J. Digit. Earth* **2018**, *13*, 602–626. [CrossRef]
28. Xu, Y.; Zhou, B.; Jin, S.; Xie, X.; Chen, Z.; Hu, S.; He, N. A framework for urban land use classification by integrating the spatial context of points of interest and graph convolutional neural network method. *Comput. Environ. Urban Syst.* **2022**, *95*, 101807. [CrossRef]
29. Fu, C.; Tu, X.; Huang, A. Identification and Characterization of Production–Living–Ecological Space in a Central Urban Area Based on POI Data: A Case Study for Wuhan, China. *Sustainability* **2021**, *13*, 7691. [CrossRef]
30. Huang, C.; Xiao, C.; Rong, L. Integrating Point-of-Interest Density and Spatial Heterogeneity to Identify Urban Functional Areas. *Remote Sens.* **2022**, *14*, 4201. [CrossRef]
31. Yang, S.; Shen, J.; Konečný, M.; Wang, Y.; Štampach, R. Study on the Spatial Heterogeneity of the POI Quality in OpenStreetMap. In Proceedings of the 7th International Conference on Cartography and GIS, Sozopol, Bulgaria, 18–23 June 2018; pp. 286–295.
32. Lin, A.; Sun, X.; Wu, H.; Luo, W.; Wang, D.; Zhong, D.; Wang, Z.; Zhao, L.; Zhu, J. Identifying Urban Building Function by Integrating Remote Sensing Imagery and POI Data. *IEEE J. Sel. Top. Appl. Earth Obs. Remote Sens.* **2021**, *14*, 8864–8875. [CrossRef]
33. Yang, X.; Ye, T.; Zhao, N.; Chen, Q.; Yue, W.; Qi, J.; Zeng, B.; Jia, P. Population Mapping with Multisensor Remote Sensing Images and Point-Of-Interest Data. *Remote Sens.* **2019**, *11*, 574. [CrossRef]
34. Zhao, B.; Tan, X.; Luo, L.; Deng, M.; Yang, X. Identifying the Production–Living–Ecological Functional Structure of Haikou City by Integrating Empirical Knowledge with Multi-Source Data. *ISPRS Int. J. Geo-Inf.* **2023**, *12*, 276. [CrossRef]
35. Fu, J.; Bu, Z.; Jiang, D.; Lin, G. Identification and Classification of Urban PLES Spatial Functions Based on Multisource Data and Machine Learning. *Land* **2022**, *11*, 1824. [CrossRef]
36. Shan, L.; Yu, A.T.W.; Wu, Y. Strategies for risk management in urban–rural conflict: Two case studies of land acquisition in urbanising China. *Habitat Int.* **2017**, *59*, 90–100. [CrossRef] [PubMed]
37. Cao, Y.; Huang, X.; Liu, X.; Cao, B. Spatio-Temporal Evolution Characteristics, Development Patterns, and Ecological Effects of "Production-Living-Ecological Space" at the City Level in China. *Sustainability* **2023**, *15*, 1672. [CrossRef]
38. Karra, K.; Kontgis, C.; Statman-Weil, Z.; Mazzariello, J.C.; Mathis, M.; Brumby, S.P. *Global Land Use/Land Cover with Sentinel 2 and Deep Learning*; IEEE: Manhattan, NY, USA, 2021; pp. 4704–4707. [CrossRef]
39. Tan, Y.; Xiong, S.; Li, Y. Automatic Extraction of Built-Up Areas from Panchromatic and Multispectral Remote Sensing Images Using Double-Stream Deep Convolutional Neural Networks. *IEEE J. Sel. Top. Appl. Earth Obs. Remote Sens.* **2018**, *11*, 3988–4004. [CrossRef]
40. Cao, F.; Qiu, Y.; Zou, Y. A fast extraction method of built-up area based on H/T breaks method and POI data. Geogr. *Geo-Inf. Sci.* **2020**, *36*, 54–60. [CrossRef]
41. Morabito, M.; Crisci, A.; Messeri, A.; Orlandini, S.; Raschi, A.; Maracchi, G.; Munafò, M. The impact of built-up surfaces on land surface temperatures in Italian urban areas. *Sci. Total Environ.* **2016**, *551*, 317–326. [CrossRef]
42. Jokar Arsanjani, J.; Helbich, M.; Bakillah, M.; Loos, L. The emergence and evolution of OpenStreetMap: A cellular automata approach. *Int. J. Digit. Earth* **2015**, *8*, 76–90. [CrossRef]
43. Liu, B.; Deng, Y.; Li, M.; Yang, J.; Liu, T. Classification Schemes and Identification Methods for Urban Functional Zone: A Review of Recent Papers. *Appl. Sci.* **2021**, *11*, 9968. [CrossRef]
44. Chen, Y.; Yang, J.; Yang, R.; Xiao, X.; Xia, J.C. Contribution of Urban Functional Zones to the Spatial Distribution of Urban Thermal Environment. *Build. Environ.* **2022**, *216*, 109000. [CrossRef]
45. Hu, S.; Gao, S.; Wu, L.; Xu, Y.; Zhang, Z.; Cui, H.; Gong, X. Urban function classification at road segment level using taxi trajectory data: A graph convolutional neural network approach. *Comput. Environ. Urban Syst.* **2021**, *87*, 101619. [CrossRef]
46. Tobler, W.R. A Computer Movie Simulating Urban Growth in the Detroit Region. *Econ. Geogr.* **1970**, *46*, 234. [CrossRef]
47. Zheng, B.; Lin, X.; Yin, D.; Qi, X. Does Tobler's first law of geography apply to internet attention? A case study of the Asian elephant northern migration event. *PLoS ONE* **2023**, *18*, e0282474. [CrossRef] [PubMed]
48. Ye, S.; Ren, S.; Song, C.; Cheng, C.; Shen, S.; Yang, J.; Zhu, D. Spatial patterns of county-level arable land productive-capacity and its coordination with land-use intensity in mainland China. *Agric. Ecosyst. Environ.* **2022**, *326*, 107757. [CrossRef]
49. Han, Z.; Shi, J.; Wu, J.; Wang, Z. Recognition Method of "The Production, Living and Ecological Space" based on POI Data and Quad-tree Idea. *J. Geo-Inf. Sci.* **2022**, *24*, 1107–1119. [CrossRef]
50. Li, C.; Wang, X.; Wu, Z.; Dai, Z.; Yin, J.; Zhang, C. An Improved Method for Urban Built-Up Area Extraction Supported by Multi-Source Data. *Sustainability* **2021**, *13*, 5042. [CrossRef]
51. Huang, M.; Wei, P.; Liu, X. An Efficient Encoding Voxel-Based Segmentation (EVBS) Algorithm Based on Fast Adjacent Voxel Search for Point Cloud Plane Segmentation. *Remote Sens.* **2019**, *11*, 2727. [CrossRef]

52. Fu, Y.; Yang, X.; Wang, T.; Supriyadi, A.; Cirella, G.T. Spatial Pattern Characteristics of the Financial Service Industry: Evidence from Nanjing, China. *Appl. Spat. Anal. Polic.* **2022**, *15*, 595–620. [CrossRef]
53. Abdulhafedh, A. Identifying vehicular crash high risk locations along highways via spatial autocorrelation indices and kernel density estimation. *World J. Eng. Technol.* **2017**, *5*, 198–215. [CrossRef]
54. Zhong, J.; Qi, W.; Dong, M.; Xu, M.; Zhang, J.; Xu, Y.; Zhou, Z. Land Use Carbon Emission Measurement and Risk Zoning under the Background of the Carbon Peak: A Case Study of Shandong Province, China. *Sustainability* **2022**, *14*, 15130. [CrossRef]
55. Guo, L.; Gong, H.; Ke, Y.; Zhu, L.; Li, X.; Lyu, M.; Zhang, K. Mechanism of land subsidence mutation in Beijing plain under the background of urban expansion. *Remote Sens.* **2021**, *13*, 3086. [CrossRef]
56. Gao, S.; Yang, L.; Jiao, H. Changes in and Patterns of the Tradeoffs and Synergies of Production-Living-Ecological Space: A Case Study of Longli County, Guizhou Province, China. *Sustainability* **2022**, *14*, 8910. [CrossRef]
57. Sun, Y.; Chang, Y.; Liu, J.; Ge, X.; Liu, G.-J.; Chen, F. Spatial Differentiation of Non-Grain Production on Cultivated Land and Its Driving Factors in Coastal China. *Sustainability* **2021**, *13*, 13064. [CrossRef]
58. Hou, D.; Meng, F.; Prishchepov, A.V. How is urbanization shaping agricultural land-use? Unraveling the nexus between farmland abandonment and urbanization in China. *Landsc. Urban Plan.* **2021**, *214*, 104170. [CrossRef]
59. Zhang, M.; Li, G.; He, T.; Zhai, G.; Guo, A.; Chen, H.; Wu, C. Reveal the severe spatial and temporal patterns of abandoned cropland in China over the past 30 years. *Sci. Total Environ.* **2023**, *857*, 159591. [CrossRef]
60. Li, C.; Zhao, J.; Xu, Y. Examining spatiotemporally varying effects of urban expansion and the underlying driving factors. *Sustain. Cities Soc.* **2017**, *28*, 307–320. [CrossRef]
61. Van Leynseele, Y.; Bontje, M. Visionary cities or spaces of uncertainty? Satellite cities and new towns in emerging economies. *Int. Plan. Stud.* **2019**, *24*, 207–217. [CrossRef]
62. Wang, M.; Derudder, B.; Liu, X. Polycentric urban development and economic productivity in China: A multiscalar analysis. *Environ. Plan. A* **2019**, *51*, 1622–1643. [CrossRef]
63. Shen, J. Universities as financing vehicles of (sub) urbanisation: The development of university towns in Shanghai. *Land Use Policy* **2022**, *112*, 104679. [CrossRef]
64. Wang, Y.; Tang, W. Universities and the formation of edge cities: Evidence from china's Government-led university town construction. *Pap. Reg. Sci.* **2020**, *99*, 245–265. [CrossRef]
65. Qiao, Z.; Liu, L.; Qin, Y.; Xu, X.; Wang, B.; Liu, Z. The Impact of Urban Renewal on Land Surface Temperature Changes: A Case Study in the Main City of Guangzhou, China. *Remote Sens.* **2020**, *12*, 794. [CrossRef]
66. Zhao, Z.; He, B.; Li, L.; Wang, H.; Darko, A. Profile and concentric zonal analysis of relationships between land use/land cover and land surface temperature: Case study of Shenyang, China. *Energy Build.* **2017**, *155*, 282–295. [CrossRef]
67. Kang, J.; Zhang, X.; Zhu, X.; Zhang, B. Ecological security pattern: A new idea for balancing regional development and ecological protection. A case study of the Jiaodong Peninsula, China. *Glob. Ecol. Conserv.* **2021**, *26*, e01472. [CrossRef]
68. Jiang, Y.; Zevenbergen, C.; Ma, Y. Urban pluvial flooding and stormwater management: A contemporary review of China's challenges and "sponge cities" strategy. *Environ. Sci. Policy* **2018**, *80*, 132–143. [CrossRef]
69. He, B.; Zhu, J.; Zhao, D.; Gou, Z.; Qi, J.; Wang, J. Co-Benefits approach: Opportunities for implementing sponge city and urban heat island mitigation. *Land Use Policy* **2019**, *86*, 147–157. [CrossRef]
70. Puma, M.J. Resilience of the global food system. *Nat. Sustain.* **2019**, *2*, 260–261. [CrossRef]
71. Qi, Y.; Chan, F.K.S.; Thorne, C.; O'Donnell, E.; Quagliolo, C.; Comino, E.; Pezzoli, A.; Li, L.; Griffiths, J.; Sang, Y.; et al. Addressing Challenges of Urban Water Management in Chinese Sponge Cities via Nature-Based Solutions. *Water* **2020**, *12*, 2788. [CrossRef]
72. Köster, S. How the Sponge City becomes a supplementary water supply infrastructure. *Water-Energy Nexus* **2021**, *4*, 35–40. [CrossRef]
73. Degirmenci, K.; Desouza, K.C.; Fieuw, W.; Watson, R.T.; Yigitcanlar, T. Understanding policy and technology responses in mitigating urban heat islands: A literature review and directions for future research. *Sustain. Cities Soc.* **2021**, *70*, 102873. [CrossRef]
74. Qu, Y.; Jiang, G.; Ma, W.; Li, Z. How does the rural settlement transition contribute to shaping sustainable rural development? Evidence from Shandong, China. *J. Rural. Stud.* **2021**, *82*, 279–293. [CrossRef]
75. Wang, Y. The Challenges and Strategies of Food Security under Rapid Urbanization in China. *Sustainability* **2019**, *11*, 542. [CrossRef]
76. Wang, Y.; Li, X.; Lu, D.; Yan, K. Evaluating the impact of land fragmentation on the cost of agricultural operation in the southwest mountainous areas of China. *Land Use Policy* **2020**, *99*, 105099. [CrossRef]
77. Yan, Y.; Yang, Q.; Zhang, H.; Zhang, R.; Yang, K.; Qu, X. The Spatial Features and Driving Mechanism of Homestead Agglomeration in the Mountainous and Hilly Areas of Southwestern China: An Empirical Study of 22 Villages in Chongqing. *Land* **2022**, *11*, 1363. [CrossRef]